SUPPLEMENT No. 408

Karppinen Tuomo - Rintala Sakari - Rantanen Antti: MV ESTONIA Accident Investigation. Numerical predictions of wave loads on the bow visor.

Technical Report VALC106. VTT Manufacturing Technology.

Espoo 1995.

MV ESTONIA ACCIDENT INVESTIGATION

Numerical predictions of wave loads on the bow visor

CONFIDENTIAL

TECHNICAL REPORT VALC106

Tuomo Karppinen, Sakari Rintala & Antti Rantanen

Espoo, December 1995

VTT MANUFACTURING TECHNOLOGY
Tekniikantie 12, Espoo, P.O.Box 1705
FIN–02044 VTT, Finland
Tel. + 358 0 4561, Fax + 358 0 455 0619, Telex 122972 vttha fi

Projekti/työ - Project identification	Sivuja - Pages	Päiväys - Date	Raportin nro - Report No.
VAL4354	44 & App.	20 December 1995	VTT VALC106

Otsikko ja tekijä - Title and author

MV ESTONIA ACCIDENT INVESTIGATION

Numerical predictions of wave loads on the bow visor

Tuomo Karppinen, Sakari Rintala & Antti Rantanen

Päivitys raporttiin nro - Update to report no.	Hyväksynyt - Approved by

Julkisuus - Availability statement — Määräpäivä - Until date

[ ] B (Julkinen - Public) [x] C (Luottamuksellinen - Confidential) [ ] C (Salainen - Secret)

Abstrakti, sisällysluettelo, tms. - Abstract, list of contents etc.

ABSTRACT

Wave loads on the bow visor of MV Estonia have been simulated in irregular head and bow seas at different forward speeds by applying a non-linear numerical method. Conclusions are based on the present estimate of the sea state, speed and heading at the time of the accident. The numerical predictions indicate that the vertical component of the wave load on the bow visor of MV Estonia may have been on the accident night quite well over 500 tons. Rough estimates of the horizontal force component and moment arm around the hinges combined with the vertical force component show that the visor opening moment may have beeen over 2 000 ton-metres. The strong dependence of the visor loads on the wave height and shape adds uncertainty in the estimates.

CONTENTS

VTT VALMISTUSTEKNIIKKA
Laiva- ja konetekniikka

VTT MANUFACTURING TECHNOLOGY
Maritime Technology

P.O. Box 1705
FIN-02044 VTT
FINLAND

Tel.int.+358 0 4561
Telefax +358 0 455 0619
Telex 122972 vttha sf

1 INTRODUCTION

The Estonian flagged passenger ferry MV Estonia encountered 28 September 1994 heavy bow seas on a scheduled voyage from Tallinn to Stockholm in the northern part of the Baltic. The lockings of the bow visor of the vessel broke and the visor fell off forcing the bow ramp open. Water flooded the car deck, the vessel lost stability and sank shortly before 2 a.m. Finnish time.

As part of the accident investigation wave loads on the bow visor of MV Estonia on the accident voyage have been estimated by a numerical method. The method and the results of the predictions are presented here. The load simulation is based on simulation of the wave-induced motions of the vessel. However, seakeeping characteristics of MV Estonia from the point-of-view of wave-induced motions are discussed in an another technical report VTT VALC53. Estimates of the sea conditions during the accident night by the Swedish, German and Finnish marine research institutes have been used in the numerical predictions.

The Swedish ship laboratory SSPA has made a systematical series of model experiments where the wave loads have been measured on bow visors different in shape than the visor of MV Estonia. Some of the results by SSPA have been compared to the numerical predictions. After the systematical series, SSPA has made wave load experiments also with a model of MV Estonia. The wave load simulations have been validated also with these test results.

Several fairly accurate methods, for instance the linear strip method (Raff, 1972), are available for predicting linear wave loads and wave-induced motions of ships in bow waves. The linear strip method, however, cannot be used for evaluating wave loads on parts of ship hull which are above the waterplane since only the underwater hull up to the mean waterline is considered in the calculations. There is no general, exact numerical method for solving the flow around a body entering water (Trosch & Kang, 1988). Due to the very complicated non-linear free surface and body boundary conditions the calculation of the impact forces on a body entering water requires simplification. Von Karman (1929) presented the first solution for this problem in two dimensions and since then several methods have been developed. A review of the solutions for circular cylinders and wedges is given by Greenhow & Yanbao (1987) and Greenhow (1987), respectively.

A practical method applied quite often for estimating the flare impact loads on ships is the non-linear strip method (e.g. Yamamoto et al. 1980). A variant of this method based on the work of Matusiak & Rantanen (1986) has been used here for simulating the vertical component of the visor load. Unfortunately the method does not give the pressure distribution on the surface of the visor and thus determination of the opening moment of the visor around the hinges must be based on quite rough estimates. On the other hand, the method is not very consuming on computer time so that it has been possible to run long simulations to find out statistics of the high visor loads.

2 CONDITIONS

2.1 Sea states

Numerical simulations of the vertical wave load on the bow visor of MV Estonia have been made in four sea states. The long-crested, irregular wave time history has been generated according to the JONSWAP wave spectrum formula given in Appendix 4. The wave spectrum shows the wave energy distribution versus frequency. In the JONSWAP spectrum, the wave energy is concentrated over a narrower frequency band than in the ISSC spectrum. The significant wave height, H_S, has been 4.0, 4.5 and 5.5 m with a modal period, T_O, of 8.0 s. The modal period is the period corresponding to the peak of the wave spectrum. In addition, a simulation has been carried out in a sea state with T_O = 8.5 s and H_S = 4.0 m. Simulations were also made in a few regular waves to compare with model test results of SSPA.

The present estimate of the sea state during the MV Estonia accident is 4 m significant height and 8 s modal period. Estimates of the modal period and the significant wave height were obtained from the Finnish, Swedish and German institutes of marine research, MTL, SMHI and DW, respectively. Table 2.1 gives their predictions determined by numerical models at the accident site at 02 Finnish time 28 September 1994, i.e. about one hour after the accident.

Table 2.1 Estimates of wave conditions at 02 28.9.1994 at the site of the accident.

Institute	H_S [m]	T_O [s]	T_1 [s]	Mean dir. [deg.]
MTL, Finland	4.4	8.2		260
SMHI, Sweden	4.2	8.5	7.2	218 - 233
DW, Germany	4.3	8.3	7.0	218

In the table, T_1 is the mean wave period. SMHI gives both the wave direction corresponding to the peak frequency (first) and the direction of the shortest waves which is the same as the wind direction. MTL and SMHI have also made estimates of the wave conditions before and after the accident. A summary of these estimates is in Table 2.2.

Table 2.2 A summary of wave conditions before and after the accident.

Institute	Position	Time	H_S [m]	T_O [s]	Mean dir.
MTL	59 25, 22 35	27.9, 23.00	3	7	260
SMHI	59 27, 22 50	27.9, 23.00	2.5	6.7	250 - 185
MTL	Accident site	28.9, 01.00	4.0	7.8	260
MTL	Accident site	28.9, 01.30	4.2	8.0	260
MTL	Accident site	28.9, 08.00	5.0	8.7	270
SMHI	Accident site	28.9, 08.00	5.1	9.5	236 - 272

The estimates of the significant wave height by the different institutes agree remarkably well. The Finnish MTL has assumed in predicting the mean wave direction that the wind shift to south on 27.9 did not last long enough to change the direction of the major wave components. This conclusion is based on their wave observations in the northern part of the Baltic. The experience of MTL is that the mean error in the predicted significant wave height is about 0.5 m, in the wave period about one second and in the wave direction about 10 degrees.

All the wave estimates are for deep water. Numerical predictions by MTL show that the significant wave height may increase significantly in shallow water due to wave focusing (Kahma et al. 1995). If waves with significant wave height 4 m and modal period 8 s enter an area where the waterdepth is around 20 m, the significant wave height may increase to 6 m while the period remains approximately constant. At the same time, statistics of the waves change so that a large part of the waves will have heights near the significant height. However, the maximum wave height will not increase respectively and remains approximately on the same level as with the original 4 m significant height.

The Finnish Lion, about 25 nautical miles west from the MV Estonia accident site, is an example of a shallow area where the significant wave height will increse in suitable weather conditions. The Finnish National Board of Navigation has analysed soundings in a sector reaching over 10 nautical miles east from the wreck of MV Estonia. The area covers the probable route of MV Estonia before the accident. The minimum waterdepth measured was 52 m which indicates that there cannot be sites shallower than about 40 m between the sounding lines. Thus, shallow waterdepth did not have an effect on the wave formation when the lockings of the bow visor of MV Estonia were broken. It may be assumed that the significant wave height was about 4 m and the modal period about 8 s at the time of the accident.

2.2 Speeds and headings

Wave loads on the bow visor have been simulated at the vessel speeds of 10, 12 and 15 knots. The present estimate of the forward speed of MV Estonia just before the accident is about 15 knots which is based on witness accounts. Simulations have been carried out in head seas corresponding to a heading angle of 180° and in bow seas at a heading of 150°. MV Estonia encountered the waves probably slightly to the port from direct head seas though there are estimates which indicate that the heading may have been closer to beam seas. The heading 150° is considered to be quite close to the actual conditions at the time of the accident.

2.3 Definition of the vessel hull form

Figure 2.1 shows the body plan and lines of MV Estonia. In the predictions of the heave and pitch Response Amplitude Operators by the SCORES-program (Raff, 1972) based on the strip method, the vessel hull form was defined by 11 and 21 sections. The number of sections had an insignificant effect on the wave-induced motions. Lewis-forms were used in defining the section shapes. Table 2.4 presents a summary of the main particulars of MV Estonia.

Table 2.4 Main particulars of MV Estonia.

	Symbol	Dimension	Value
Length over all	L_{oa}	m	155.4
Waterline length	L_{wl}	m	144.8
Length betw. perp.	L_{pp}	m	137.4
Beam mld, A deck	B	m	24.2
Waterline beam	B_{wl}	m	23.6
Draught at aft. perp.	T_a	m	5.75
Draught at forw. perp.	T_f	m	5.25
Trim, positive by stern		m	0.50
Displacement	V	m^3	12 243
Longitudinal CG from aft. perp.	LCG	m	63.7
Vertical CG	KG	m	10.50
Transverse metacentric height	GM_T	m	1.28
Roll radius of gyration	k_{xx}	m	8.96
Pitch radius of gyration	k_{yy}	m	36.2
Depth to stemhead	D	m	10.0

The numerical predictions are for a vessel mean draught of 5.5 m and an aft trim of 0.5 m, i.e. the draft at the forward perpendicular was 5.25 m and at the aft perpendicular 5.75 m. The displacement of 12 365 tons at a water density of 1.01 tons/m^3 and the longitudinal centre of gravity were taken from hydrostatic calculations by the NAPA-program. After the predictions had been made, the load condition of MV Estonia during the accident trip was estimated as 12050 tons and 0.435 aft trim. The fore and aft draughts are respectively 5.172 m and 5.607 m. The difference between the actual and the assumed loading condition is so small that it has hardly any effect on the wave-induced motions.

Standard values of $0.25L_{wl}$ and $0.38B_{wl}$ were used for the longitudinal and transverse radius of gyration, respectively. The transverse metacentric height was set to 1.3 m while the actual value was 1.17m. Also the actual location of the centre of gravity differed a little from the assumed value. The final estimated values are: LCG = 63.85 and KG = 10.62 m. A summary of the input data is given in Appendix 3.

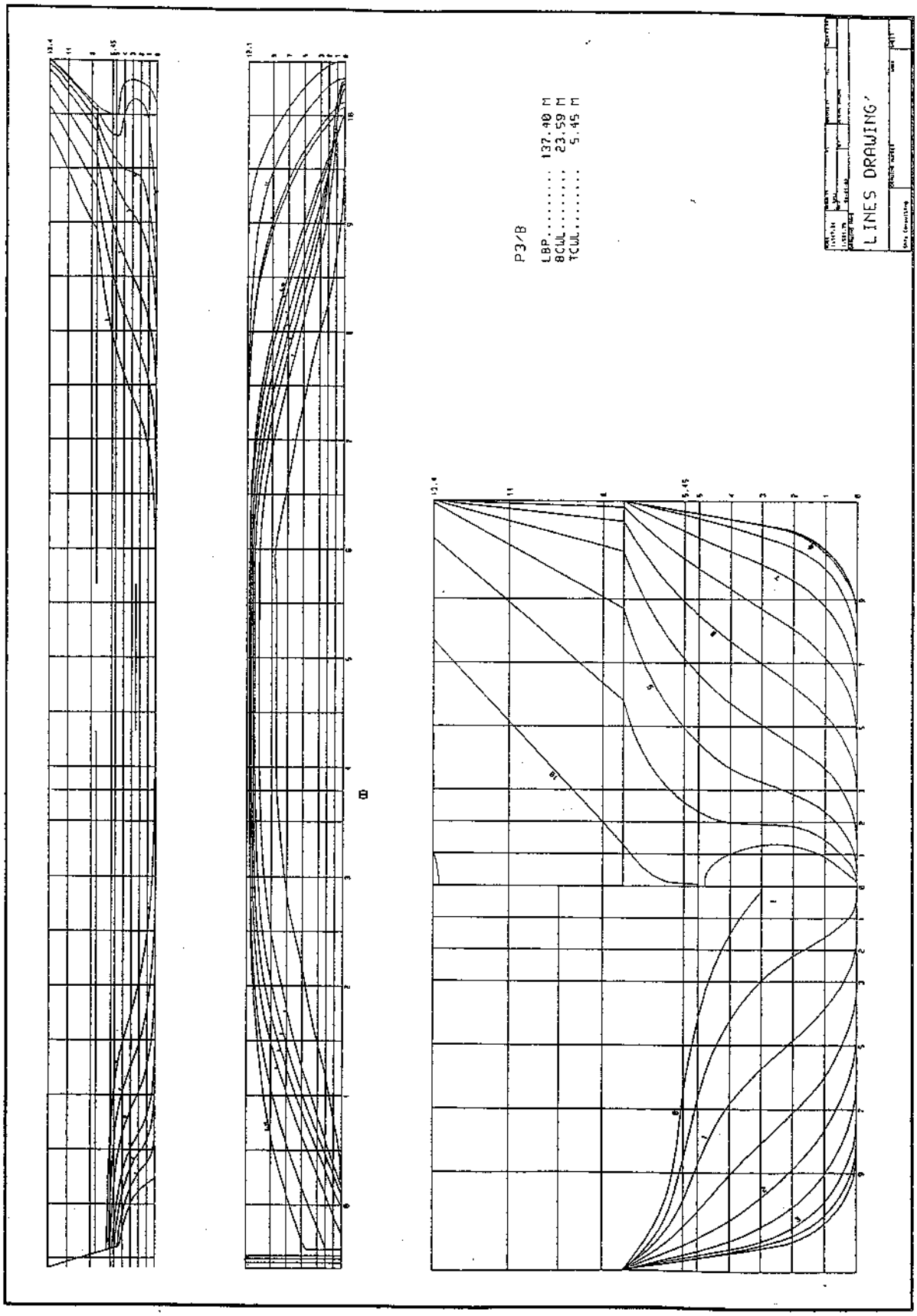

Fig. 2.1 Body and lines plan of MV Estonia.

VTT VALMISTUSTEKNIIKKA
Laiva- ja konetekniikka
VTT MANUFACTURING TECHNOLOGY
Maritime Technology
P.O. Box 1705
FIN-02044 VTT
FINLAND
Tel.int.+358 0 4561
Telefax +358 0 455 0619
Telex 122972 vttha sf

3 SIMULATION METHOD

The simulation method is based on the so called non-linear strip theory (Yamamoto et al., 1980 and Chiu & Fujino, 1991) which is a practical method for simulating ship motions in waves. A main difference between the linear strip method and the non-linear strip method is that in the linear theory the equations of motion are solved for the mean waterline in the frequency domain while in the non-linear version the motions are simulated in the time domain and the non-linearities of the hydrodynamic forces arising from the variation of the submerged portion of the hull are taken into account. Here the formulas of the non-linear strip method have been applied for simulating the vertical force on the bow visor in long-crested, irregular waves. However, the rigid body wave-induced motions of the ship have been determined by the linear strip method (Raff, 1972) and simulated by applying the linear superposition principle. The approach is based on the work of Matusiak & Rantanen (1986). The non-linearities in the hydrodynamic forces affect only slightly heave and pitch (Yamamoto et al. 1980).

The non-linear hydrodynamic forces on a heaving ship section may be determined by a momentum consideration as shown by Faltinsen (1990). The method has been widely applied for predicting the hydrodynamic forces on prismatic bodies entering water (e.g. Payne, 1981, and Greenhow, 1987) and for instance by Gran et al. (1976) for estimating the hydrodynamic impact forces on a bow with large flare. Here the bow visor has been considered as a small body entering water. The non-linear forces arising from the momentum consideration and the hydrostatic and hydrodynamic forces as defined in the strip theory (Raff, 1972) are taken into account. However, the term involving the longitudinal derivative of the sectional heave added mass has been neglected. This simplification has probably a minor effect on the results. The instantaneous waterplane has been used for determining the added mass, damping and hydrostatic coefficients of the bow visor. All viscous and memory effects have been disregarded.

3.1 Irregular waves

In the simulations, time histories of irregular waves, surface velocities and accelerations are generated by applying the linear superposition principle, i.e. a large number of regular sinusoidal wave components are summed (Fig.3.1). The amplitude of a regular wave component at frequency ω is determined on the basis of the ordinate of the simulated wave spectrum at ω. In order to get non-repeating random time histories of arbitrary length, each harmonic wave component has a random phase angle and its frequency ω is chosen at random in each narrow frequency band.

The elevation of a long-crested wave surface, η, as a function of time, t, is expressed by:

$$\eta(t) = \sum_{i=1}^{N} a_i \cos(k_i X \cos\mu + k_i Y \sin\mu - \omega_i t + \varepsilon_i) \qquad (1)$$

where

a_i = Amplitude of the ith harmonic wave component
ω_i = Circular frequency of the ith harmonic wave component
ε_i = Random phase angle of the ith wave component
k_i = Wave number of the ith wave component
μ = Angle of wave propagation with regard to the positive X-axis

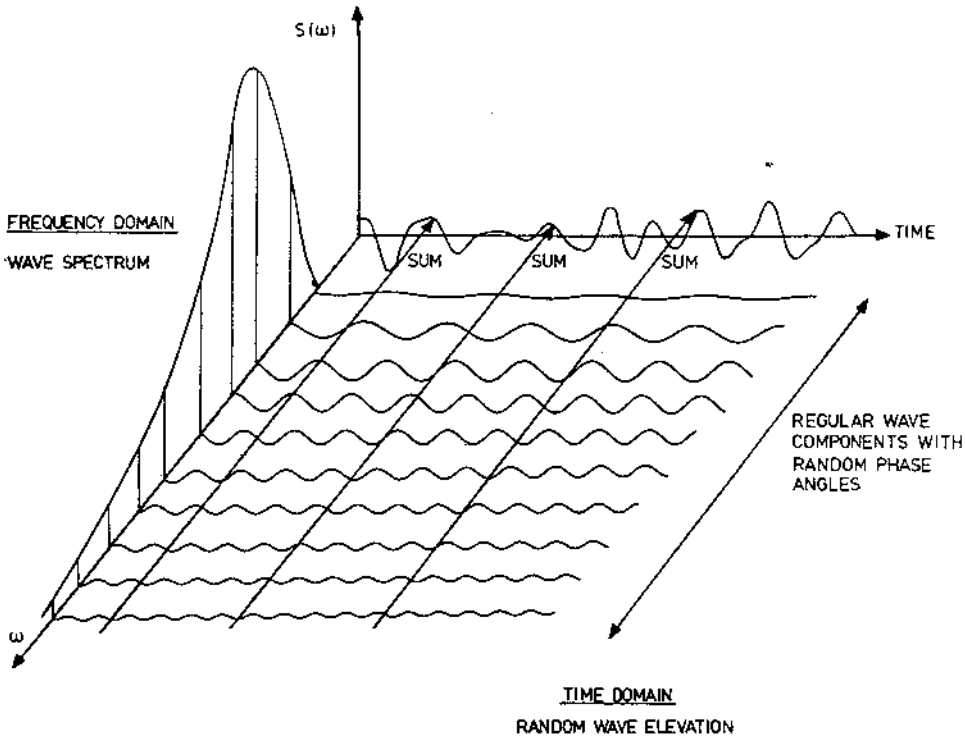

Fig. 3.1 The superposition principle (Faltinsen, 1990).

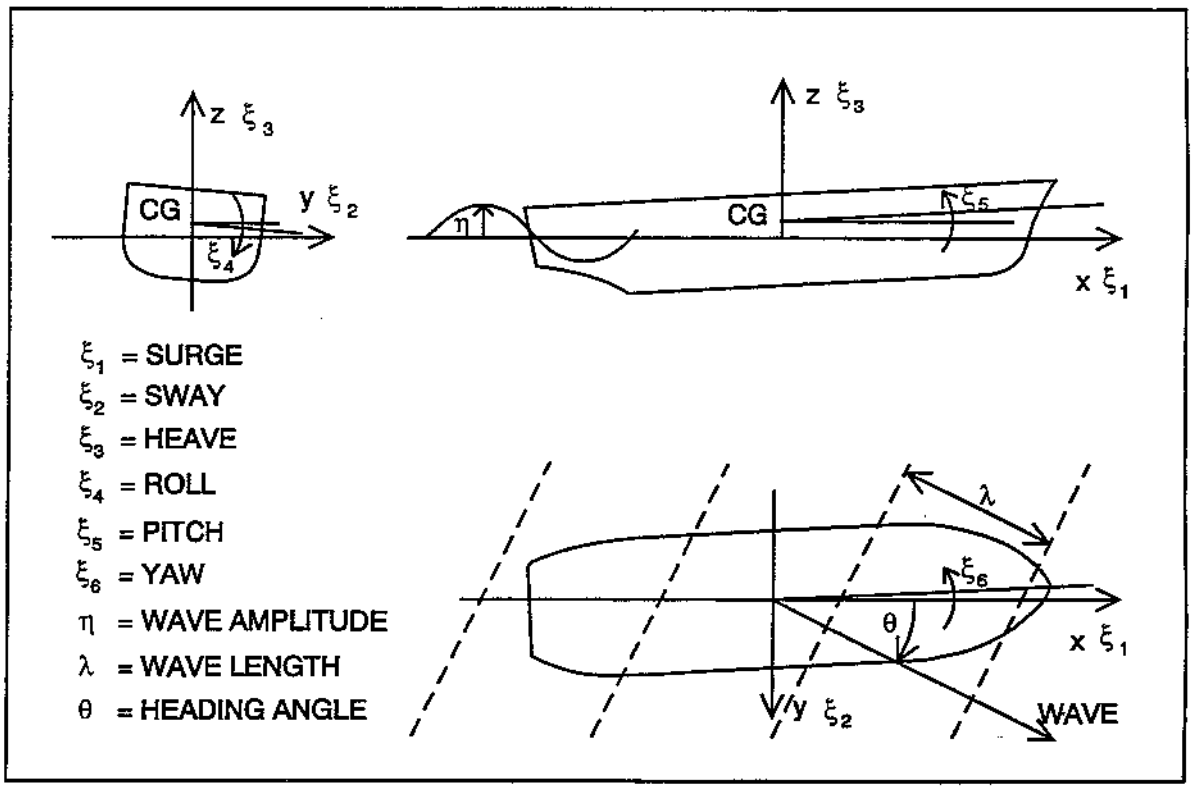

Fig. 3.2 Axis system and definitions.

The wave surface elevation (1) is defined in a Cartesian coordinate system (X,Y,Z) where the origin is fixed to the undisturbed free water surface defined by Z = 0. The positive direction of Z points upwards. The equation (1) may be transformed to a reference frame moving with the steady forward motion of the ship just by replacing the circular frequency of the ith harmonic wave component by the frequency of encounter:

$$\omega_{ei} = \omega_i - k_i V \cos\mu \qquad (2)$$

where V is the steady forward speed of the ship. The origin of the moving reference frame (x,y,z) (Fig. 3.2) translates in the XY-plane with speed V so that the centre of gravity of the ship is in rest position on the vertical z-axis. The ship moves in the positive x-direction which coincides with the earth-fixed X-direction.

In deep water, the wave number is given by $k = \omega^2/g$ where g is the acceleration due to gravity. The vertical velocity and acceleration of the wave surface are obtained as the first and second time derivative of (1), respectively.

The ramdomness of the phase lags implies that there is an equal probability of their having any value between 0 and 2π. The amplitude a_i of the ith wave component is determined by:

$$a_i = \sqrt{2S(\omega_i)\Delta\omega} \qquad (3)$$

where

$S(\omega_i)$ = Ordinate of the simulated wave spectrum at frequency ω_i

$\Delta\omega$ = Frequency increment

The wave time histories have been simulated according to the JONSWAP spectrum. The number of regular wave components used in generating the wave time histories has been 20. This should give an adequate representation of the wave field without lengthening too much the computer time required by the simulation. The high-frequency end of the wave spectrum has been cutted out at ω = 1.72 rad/s to have only wave components with length large relative to the dimensions of the bow visor. In this way the assumption of constant water particle velocity and acceleration over the space occupied by the visor is fulfilled. The high-frequency components have an insignificant effect on the significant wave height but may increase the velocity and acceleration unrealistically.

3.2 Wave-induced motions

Heave and pitch (Fig. 3.2) in the simulated irregular long-crested seas are obtained by determining first the responses to each regular wave component on the basis of heave and pitch response amplitude operators and phase lags predicted by the strip method (Raff, 1972). Summing the heave and pitch responses to the regular wave componets gives the time histories in the form:

$$\xi_j(t) = \sum_{i=1}^{N} \left| R_j(\omega_{ei}) \right| a_i \cos(k_i x \cos\mu + k_i y \sin\mu - \omega_{ei} t + \alpha_j(\omega_{ei}) + \varepsilon_i) \quad \text{for j = 3 and 5} \qquad (4)$$

where ξ_j for j = 3 and 5 are heave and pitch, respectively, R_j for j = 3 and 5 are the heave and pitch transfer functions, respectively, i.e. the response amplitude per unit wave amplitude, and α_j are the heave and pitch phase lags with regard to the wave crest at the origin. The transfer functions and the phase lags depend on the frequency of oscillation, or the frequency of encounter.

During the simulation, at each time step the vertical relative displacement, relative velocity and relative acceleration at the bow visor are determined as the difference between the rigid body vertical displacement, velocity, and acceleration, and the wave surface displacement, velocity and acceleration, respectively. The undisturbed, incident wave surface (1) is used. The vertical relative motion at the bow visor is given by:

$$\xi_r(t) = \eta - \xi_3 - x_b\xi_5 \qquad (5)$$

where x_b is the longitudinal coordinate of the centre of the bow visor. Here heave is assumed positive upwards and pitch positive bow up. The vertical relative velocity may be expressed as:

$$\dot{\xi}_r(t) = \dot{\eta} - \dot{\xi}_3 - x_b\dot{\xi}_5 + V\xi_5 \qquad (6)$$

where the dots indicate time derivative. The vertical relative acceleration is obtained as a time derivative of (6).

3.3 Vertical force on the visor

The total vertical force component on the visor is predicted by:

$$F_Z = F_i + F_{rd} + F_S + F_{FK} + F_{imp} + F_{st} - m_V g \qquad (7)$$

where

F_i = Inertia force
F_{rd} = Linear radiation plus diffraction force
F_S = Hydrostatic, or displacement force
F_{FK} = Froude-Krylov force
F_{imp} = Non-linear hydrodynamic impact force
F_{st} = Vertical component of the hydrodynamic force due to the stationary flow
m_V = Mass of the visor = 60.000 kg
g = Acceleration due to the gravity

The inertia force F_i is obtained as the mass of the visor, m_V, times the rigid body vertical acceleration of the ship at the centre of the visor:

$$F_i = -m_v(\ddot{\xi}_3 + x_b\ddot{\xi}_5) \qquad (8)$$

The centre of the visor has been assumed to locate at a distance of 3.44 m forward of FP.

The linear radiation plus the diffraction force is determined by:

$$F_{rd} = m_{33}(t)\ddot{\xi}_r + b_{33}(t)\dot{\xi}_r \qquad (9)$$

where

m_{33} = heave added mass of the visor up to the instantaneous wave surface
b_{33} = heave damping coefficient of the visor up to the instantaneous wave surface

3.3.1 Added mass and damping coefficients

The heave added mass and damping coefficients of the visor at different waterlines have been computed by a three-dimensional sink-source method (Kalske et al., 1985) which is based on the numerical algorithm developed by Garrison (1974). In these numerical predictions, the surface of the visor has been described by triangular elements (Fig. 3.3). Different numbers of elements have been used at different draughts according to Table 3.1. The shape of the visor has been simplified so that the back bulkhead is vertical and the lower end is sharp (Fig. 3.4). Thus, the original visor has more volume at the lower end than the model used in the simulations. Higher up the difference in volume equalizes.

Table 3.1 Number of elements.

Draught [m]	Elements
7	5
9	24
11	55
13	98
15.4	153

The sink-source method is based on the linear potential flow theory. The velocity potential describing the flow due to the oscillatory motion of the body in six degrees of freedom is obtained as a solution of the Laplace's equation in the fluid domain bounded by the wetted body surface, the free fluid surface and a possible horizontal bottom. In this case, the fluid depth has been assumed infinite. The velocity potential satisfies on the free surface the linear, zero-speed boundary condition and on the body surface the condition of no flow through the surface, i.e. the fluid velocity and the velocity of the surface into the direction normal to the surface are equal. Due to linearization, which is based on the assumption of small motions, the boundary conditions are applied on the plane of the mean free surface and at the mean position of the body. In addition, the velocity potential satisfies a radiation condition of outgoing waves. The added mass and damping coefficients are obtained from the velocity potential.

The predictions were made for three frequencies, f = 0.172, 0.208 and 0.263 Hz covering the range of wave encounter frequencies with the major wave components. The oscillation frequency had a small effect on the results. The largest values of the coefficients have been used in the simulations. Figure 3.5 shows that the added mass versus draught follows closely the displaced volume of the visor. The added mass and damping coefficients were given as input in tabular form to the simulation program and curve fitted by a third degree polynomial. At each time step, the added mass and damping coefficients have been determined for the instantaneous draught by using the curve fitted values.

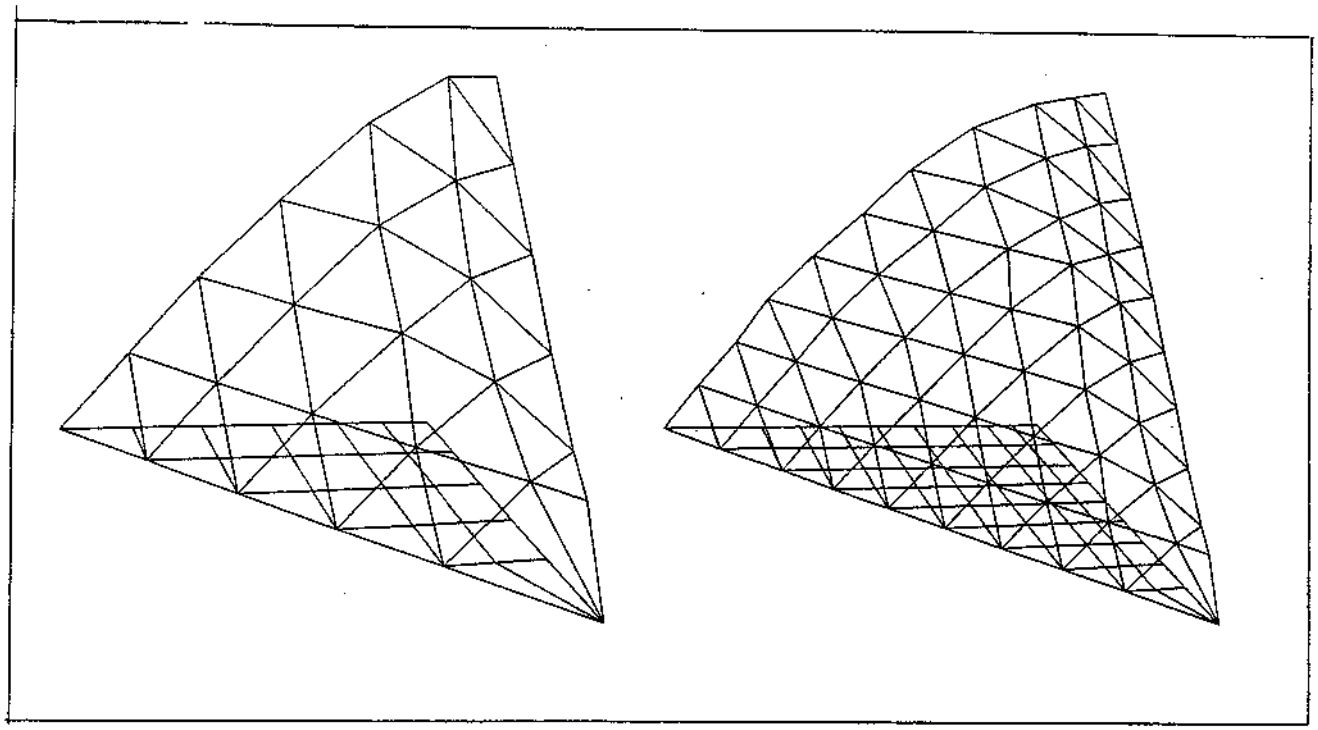

Fig. 3.3 Element mesh of the visor at 11 m and 15.4 m (right) draughts.

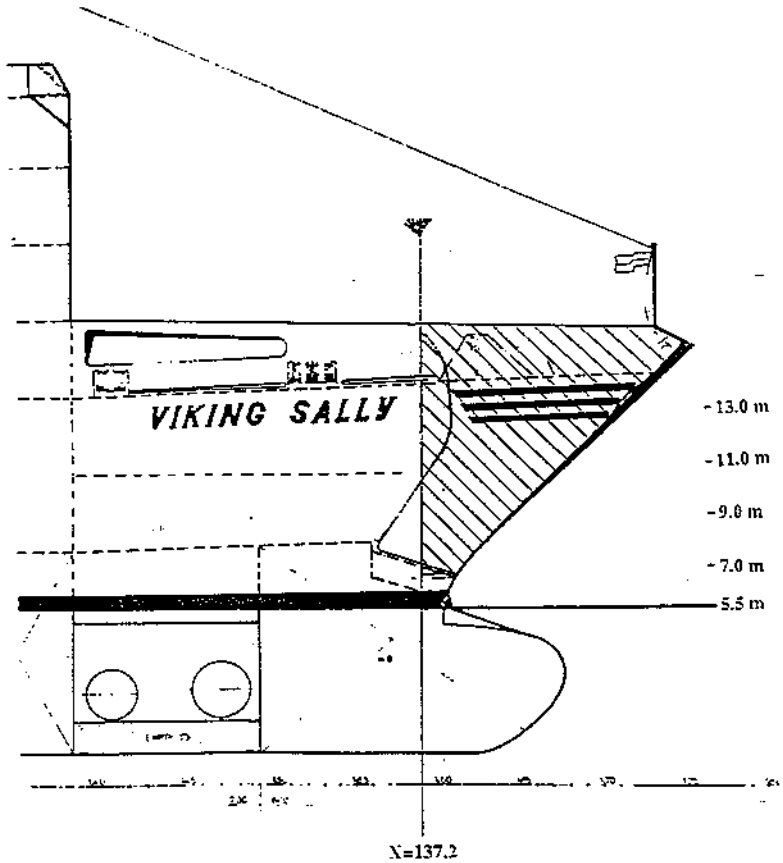

Fig. 3.4 The simplified shape of the visor used in the numerical predictions.

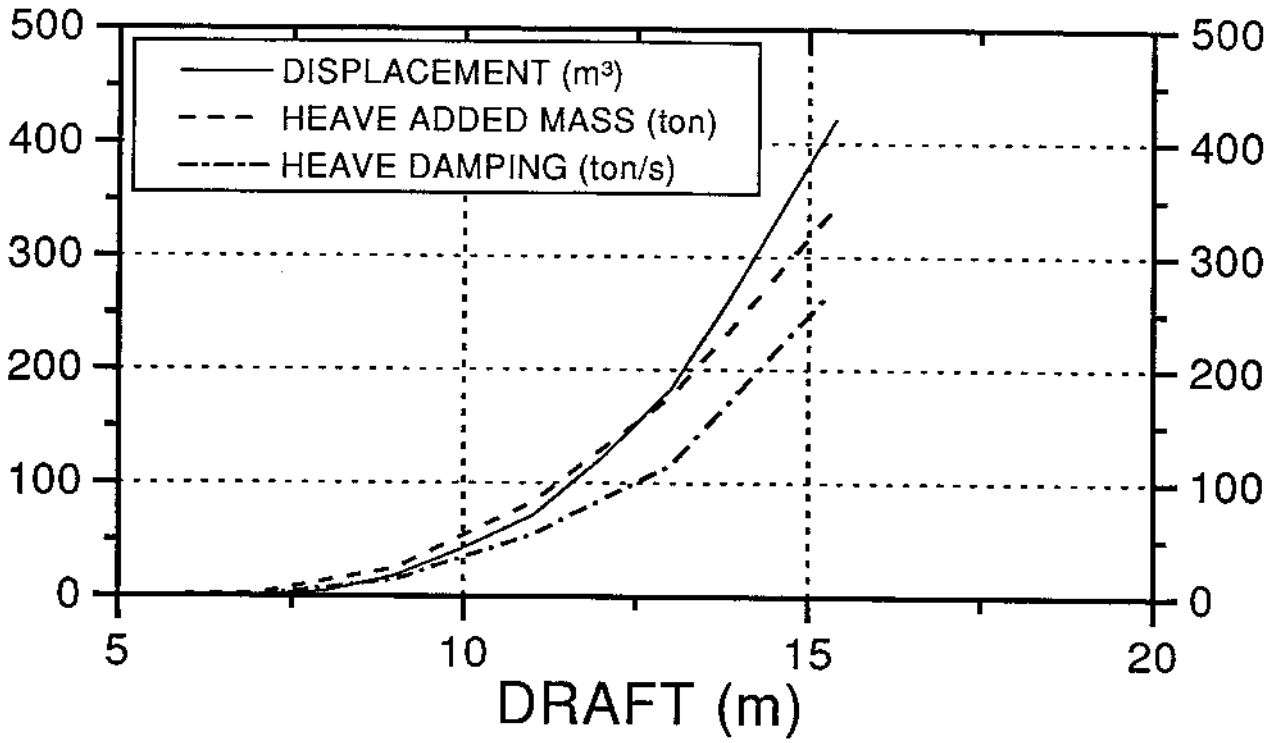

Fig. 3.5 Displacement, heave added mass and damping of the visor versus draught.

3.3.2 Hydrostatic and Froude-Krylov force

The vertical component of the hydrostatic plus the Froude-Krylov force is given by (de Kat & Paulling, 1989):

$$F_s + F_{FK} = \iint_S (p_s + p_d) n_z dS \qquad (10)$$

where

p_s = Hydrostatic pressure = ρgz

p_d = Dynamic pressure in the undisturbed, incident wave

n_z = Vertical component of the unit normal to the body surface

The intergration is carried out over the instantaneous total wetted surface. Thus, in the expression of the hydrostatic pressure, z is the height of the water column up to the wave surface, η(t). In the simulation, the hydrostatic force is expressed as:

$$F_S = \rho g \nabla_V(t) \qquad (11)$$

where

ρ = Water density

∇_V = Instantaneous submerged volume of the visor

The Froude-Krylov force is defined as the force that is obtained by integrating the pressure in the undisturbed, incident wave over the wetted surface of the visor. Thus, it is assumed that the ship

does not disturb the incident wave. The wave pressure determined by the linearized Bernoulli's equation in the moving reference frame is given by:

$$p_d = \rho g \sum_{i=1}^{N} a_i \exp(k_i z) \cos(k_i x \cos\mu + k_i y \sin\mu - \omega_{ei} t + \varepsilon_i) \qquad (12)$$

In the linearized wave theory, the free fluid surface is defined as the plane z = 0. Using this approximation in (12) yields for the dynamic pressure near the wave surface:

$$p_d = \rho g \eta(t) \qquad (13)$$

Assuming further that the pressure variation in the horizontal plane within the dimensions of the bow visor may be neglected, the vertical component of the Froude-Krylov force on the visor may be expressed as:

$$F_{FK} = \rho g A_{wv}(t) \eta(t) \qquad (14)$$

where

A_{WV} = Instantaneous waterplane area of the visor

Thus, the undisturbed, dynamic wave pressure has been assumed constant over the surface of the visor. This assumption is consistent with the assumption of small dimensions of the visor compared to the wave length. A similar approach has been used by Hooft (1970), Karppinen (1975) and many others for estimating the wave loads on small structural members of offshore structures. The method is thoroughly discussed by Newman (1977). Consistent with this approach is that in the simulation the vertical relative velocity and acceleration are determined at the centre of the visor, at the station 3.44 m forward of FP on the sea surface.

3.3.3 Non-linear impact force

The non-linear impact force is expressed in the form:

$$F_{imp} = \frac{\partial m_{33}}{\partial z} \dot{\xi}_r^2 + \frac{\partial b_{33}}{\partial z} \xi_r \dot{\xi}_r \qquad (15)$$

The impact force consists of two parts the one of which is proportional to the vertical rate of change of the added mass and the other to the rate of change of the damping. The term involving the derivative of the damping coefficient is much smaller than the added mass term which is proportional to the relative vertical velocity squared. At each time step, the values of the coefficients and the relative motion and velocity are updated.

3.3.4 Force due to the stationary flow

The final term in the force equation takes into account the effect of the stationary flow when the bow pitches down to the water. The pressure distribution on the bow in calm water at different fore draughts has been computed by the SHIPFLOW- program at 10, 15 and 20 knots speed of the vessel (Sundell, 1995). An integration of the pressure over the visor area up to the bow wave surface yields the vertical and horizontal component of the force on the visor while an integration of the horizontal pressure component over the total wetted surface of the ship would give the wave

resistance. The vertical force component on the visor has been programmed to the simulation method as a simple function giving the force versus the draught at FP (Fig. 3.6).

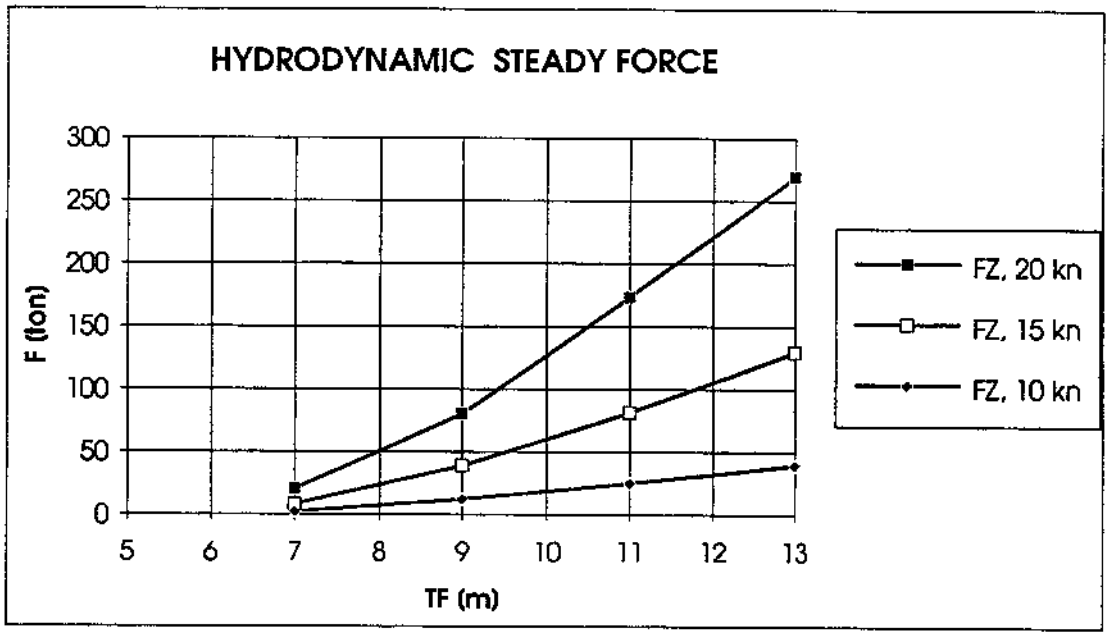

Fig. 3.6 The effect of ship speed and bow submergence on the steady, vertical, hydrodynamic force.

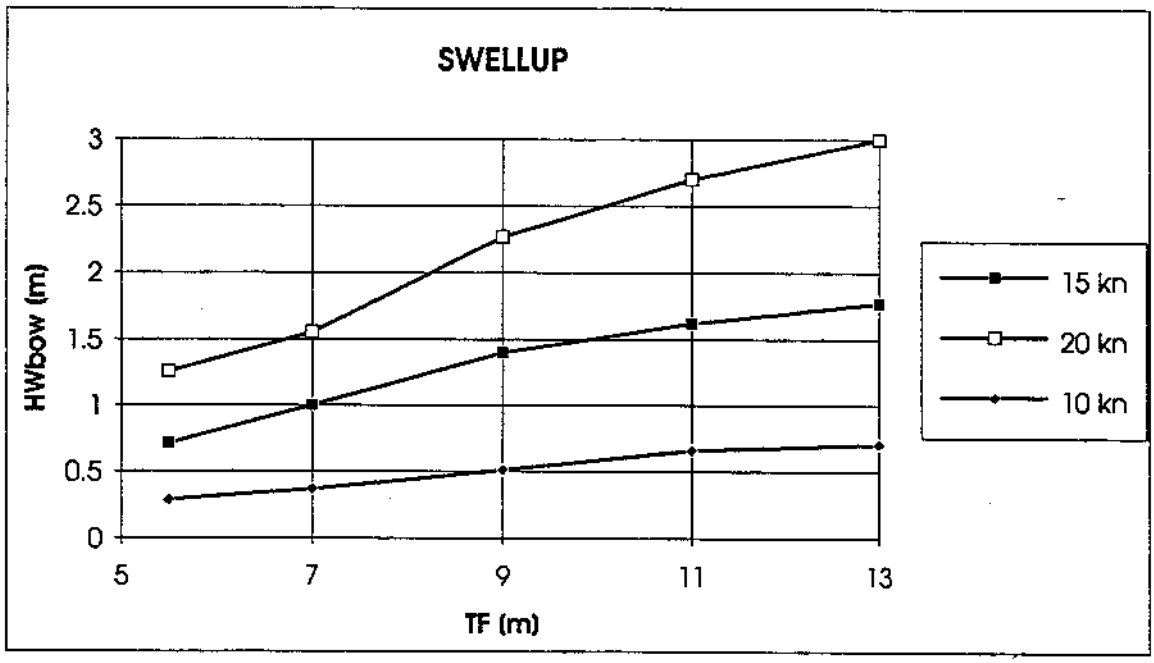

Fig. 3.7 The bow wave height as a function of draught at FP and ship speed.

The SHIPFLOW program is a general program package for predicting the flow around a ship hull and the corresponding forces in still water, in particular the resistance of the ship. The development, basic principles of the solution method and the application of the program are described by Larsson et al (1990) and Larsson (1993). The potential flow part of the program has been used for estimating the forces on the visor. In the potential flow method, the hull surface and part of the free surface are discretized by panels using Rankine sources. The source strengths are determined so that the boundary conditions are satisfied. The program has been run using both the linear and the non-linear version of the free surface boundary condition.

Figure 3.6 shows that the vertical force due to the stationary flow increases quickly with inceasing speed and forward draught. At a large bow submergence, the force is about 100 tons at 15 kn speed and over 200 tons at 20 kn speed. The large force at 20 kn speed is due to the bow wave height rising to over 3 m high. The numerical method does not model wave breaking which would probably take place before the wave grows so high. At 15 kn speed, the bow wave height is 1 to 1.5 m. The predictions are for a steady situation while in waves the bow is pitching up and down at the quite short wave encounter period. It is questionable whether the bow wave rises to the same height during this pitch period as in calm water in a steady flow. However, the predictions by the SHIPLOW-program have not been tried to correct for these effects. On the other hand, the effect of the horizontal water particle velocity in the incoming wave has been disregarded and only the stationary flow due to the vessel forward speed has been considered in the predictions. The neglected effect of the horizontal water particle velocity, in particular if waves are breaking, probably more than compensates for the effect of a too high bow wave.

The bow wave has also the important effect of decreasing the freeboard, or helping lower waves to reach the visor. Since the displacement and the waterplane area of the visor increase dramatically higher up (Fig. 3.5), the bow wave height may have a significant effect on the wave loads of the visor. In the simulations, the bow wave has been considered as a constant offset increasing the submergence of the visor. Thus, the height of the bow wave has been added to the relative motion. In reality, there must be interaction between the bow wave, incoming wave and the waves generated by ship motion so that the simple superposition does not strictly hold. A proper numerical method would give the behaviour of the bow wave as part of the solution.

4 RESULTS

Main results of the simulations are curves presenting probabilites at which the vertical component of the wave force on the visor exceeds different levels. Table 4.1 gives a summary of the figures showing curves of exceedance probabilities. The exceedance probabilities are plotted on a logarithmic scale while the vertical force is on a linear scale. In this form, straight lines seem to fit the data quite well for high load values. There is no theoretical basis for the linear relationship between the logarithm of the exceedance probability and the vertical visor load. In many cases, for instance the long-term distributions of wave heights and hull wave bending moments, the Weibull-distribution gives a good fit to the data.

The wave load on the bow visor is highly non-linear with regard to the wave amplitude and the statistical distribution of the loads is not known. Since the distibution is unknown, long simulations have been made to get relatively accurate estimates for the extreme load values. The simulated sequences have been 36 hours long in which time the vessel encountered about 30 000 waves

depending on the speed, heading to waves and wave period. The simulations were carried out in each case in six six hours long runs. The vessel encountered thus in one hour about 1 000 waves. If the probability of exceeding a certain vertical force level is 0.001, for instance, then in the mean one in 1 000 waves encountered causes a vertical wave load on the visor exceeding the level in question. The highest load value in the 36 hours long simulation has an exceedance probability of about 1/30 000. Table 4.2 shows a summary of the wave encounters in 24 hours when T_O = 8.0 s.

Table 4.1 Summary of figures showing exceedance probabilities of visor loads.

Heading [deg.]	Bow wave height [m]	Speed [kn]	H_S [m]	T_O [s]	Figure number
Head seas, 180	1.0	15	4.0	8.0	5.4
Head seas	1.0	15	4.0	8.5	5.5
Head seas	0.65	12	4.0	8.0	5.4
Head seas	0.4	10	4.0	8.0	5.4
Head seas	0.4	10	5.5	8.0	5.6
Head seas	0.65	12	5.5	8.0	5.6
Head seas	1.0	15	5.5	8.0	5.6
Head seas	1.5	15	5.5	8.0	5.7
Bow seas, 150	1.0	15	4.0	8.0	5.8
Bow seas	1.0	15	4.5	8.0	5.8
Bow seas	1.5	15	4.0	8.0	5.8

Table 4.2 Number of wave encounters in 24 hours when T_O = 8.0 s.

	Speed [kn]		
Heading	10	12	15
180 deg.	18 600	20 000	23 200
150 deg.			20 700

The distribution of peak load values, the maximum peak per one wave encounter period, has been determined for every six hours long simulation. Also the distribution of all the load data, one value taken at each time step, has been determined. Time histories of the four highest positive and negative load peaks and waves have been plotted. The highest positive load peak in every six hours long simulation has been analysed more closely to show the magnitudes of the different load components. The wave and the vertical relative motion at the bow visor which caused the maximum load have also been plotted.

Wave surface elevation, vertical relative motion and the vertical wave load components on the visor plotted at the same time for a short time sequence are given in the same figure. Table 4.3 presents a summary of the figures showing selected time histories of wave elevation, relative motion and wave load components.

Table 4.3 Summary of figures showing sequencies of wave, relative motion and load components.

Heading [deg.]	Bow wave height [m]	Speed [kn]	H_S [m]	T_O [s]	Cases	Figures
Head seas, 180	1.0	15	4.0	8.0	1, 3, 5	A1.1 - A1.3
Head seas	1.0	15	4.0	8.5		
Head seas	0.65	12	4.0	8.0		
Head seas	0.4	10	4.0	8.0		
Head seas	0.4	10	5.5	8.0		
Head seas	0.65	12	5.5	8.0	2, 4, 5	A1.4 - A1.6
Head seas	1.0	15	5.5	8.0	2, 4, 5	A1.7 - A1.9
Head seas	1.5	15	5.5	8.0		
Bow seas, 150	1.0	15	4.0	8.0	2, 3, 6	A1.10 - A1.12
Bow seas	1.0	15	4.5	8.0	2, 3, 6	A1.13 - A1.15
Bow seas	1.5	15	4.0	8.0		

All the figures in Appendix 1 show incidents of high vertical loads on the visor. The case number in the figures refers to a specific six hours long simulation. The upper plot in the figures presents the simulated wave elevation and the vertical relative motion as a function of time. On the vertical axis, the zero level corresponds to the mean freee surface, i.e. to the still water level. The relative motion computed by formula (5) is the submergence (positive) or emergence (negative) of the bow measured from the mean waterplane. The relative motion given in the figures does not include the bow wave height which has been added to the motion before predicting the wave load on the visor.

The lower plot in the figures shows the most important components of the vertical wave load on the visor. The inertia force is the added mass of the visor times the vertical relative acceleration, i.e. the first part of the force given by formula (9). The buoyancy force includes both the hydrostatic and the Froude-Krylov force predicted by formulas (11) and (14), respectively. The slamming force has been computed by (15), and finally the total force by (7).

Figures showing selected peak and level distributions of waves and visor loads are given in Appendix 2. The distributions are from specific six hours long simulations. The following table summarises the visor load distributions.

Table 4.4 Summary of figures showing peak and level distributions of loads.

Heading [deg.]	Bow wave height [m]	Speed [kn]	H_S [m]	T_O [s]	Cases	Figures
Head seas, 180	1.0	15	4.0	8.0	1, 3, 5	A2.4 - A2.6
Head seas	0.65	12	5.5	8.0	2, 4, 5	A2.7 - A2.9
Head seas	1.0	15	5.5	8.0	2, 4, 5	A2.10 - A2.12
Bow seas, 150	1.0	15	4.0	8.0	2, 3, 6	A2.13 - A2.15
Bow seas	1.0	15	4.5	8.0	2, 3, 6	A2.16 - A2.18

5 DISCUSSION

Figures 5.1 and 5.2 show short sequencies of simulated irregular waves and wave loads on the bow visor, respectively. The wave time history includes a wave crest of about 5 m high but otherwise the record seems to be approximately symmetric about the still water level, i.e. the heights of crests and troughs follow the same distribution. The wave load record is highly asymmetric showing only high positive peaks due to the bow submergence. Low waves don't even reach the visor and the vertical force on the visor remains close to its weight of 600 kN. Both the wave and the load record have time scales as the vessel encounters head waves at 15 knots speed.

Time histories of high vertical loads on the visor are given in Appendix 1. The figures show also the wave and the relative motion which caused the high load. The vertical load increases quickly, in about 0.1 s, to a high value which is almost entirely due to the impact force term, or the term proportional to the relative velocity squared. Then also the hydrostatic plus the Froude-Krylov force becomes important and at the maximum load value this "buoyancy" force is approximately equally large as the impact force. The added mass inertia force acts to the opposite direction and decreases the total force. The inertia force has its minimum and the Froude-Krylov force its maximum when the relative motion has the maximum, i.e. the bow is deeply submerged. This occurs approximately when the wave crest passes the visor. The impact force oscillates on a high level about half a second and drops then down. The oscillations seem to be due to the numerical derivation of the visor added mass and have thus no physical origin. The impact force is nearly zero at the maximum of relative motion. In all cases of high loads, the time histories of the load components follow approximately the same pattern.

At the same speed and heading, the same individual waves excite the high loads regardless of significant wave height since the wave time histories have been generated by linearly scaling six basic six hours long time histories in the case of $T_0 = 8.0$ s. This becomes evident by comparing the wave elevations in Figures A1.3 and A1.9 and Figures A1.10 - A1.12 to Figures A1.13 - A1.15. The wave time histories with a modal period of 8.5 s have a different shape than with $T_0 = 8$ s. When the vessel speed or heading is changed, different individual waves of the same wave time history cause the highest loads on the visor.

Often high loads seem to be excited by waves which have a flat trough and a steep front. The crest following the trough may be twice as high as the through is deep. Deep wave troughs, even followed by a relatively high crest, seem to never excite high loads on the visor. Waves associated with the largest loads are not necessarily the highest. Of the four highest load peaks in one six hours long simulation, usually one ore two load peaks are associated with the four highest wave crests in the wave time history. It seems thus that waves with only a small differences in the shape may excite significantly different loads on the visor. This is illustrated by Figure 5.3 where the wave in the upper plot excited on the visor a vertical force of 9 800 kN and the lower a force of only under 5 200 kN in head seas with $H_s = 5.5$ m at a speed of 15 kn. It would be interesting to analyse more closely characteristics of a short sequence of waves preceeding a high load on the visor and try to relate the wave characteristics to the load. Kagemoto et al. (1995) show that a group of high successive waves may induce a significantly larger motion displacement for a floating body than just one high wave.

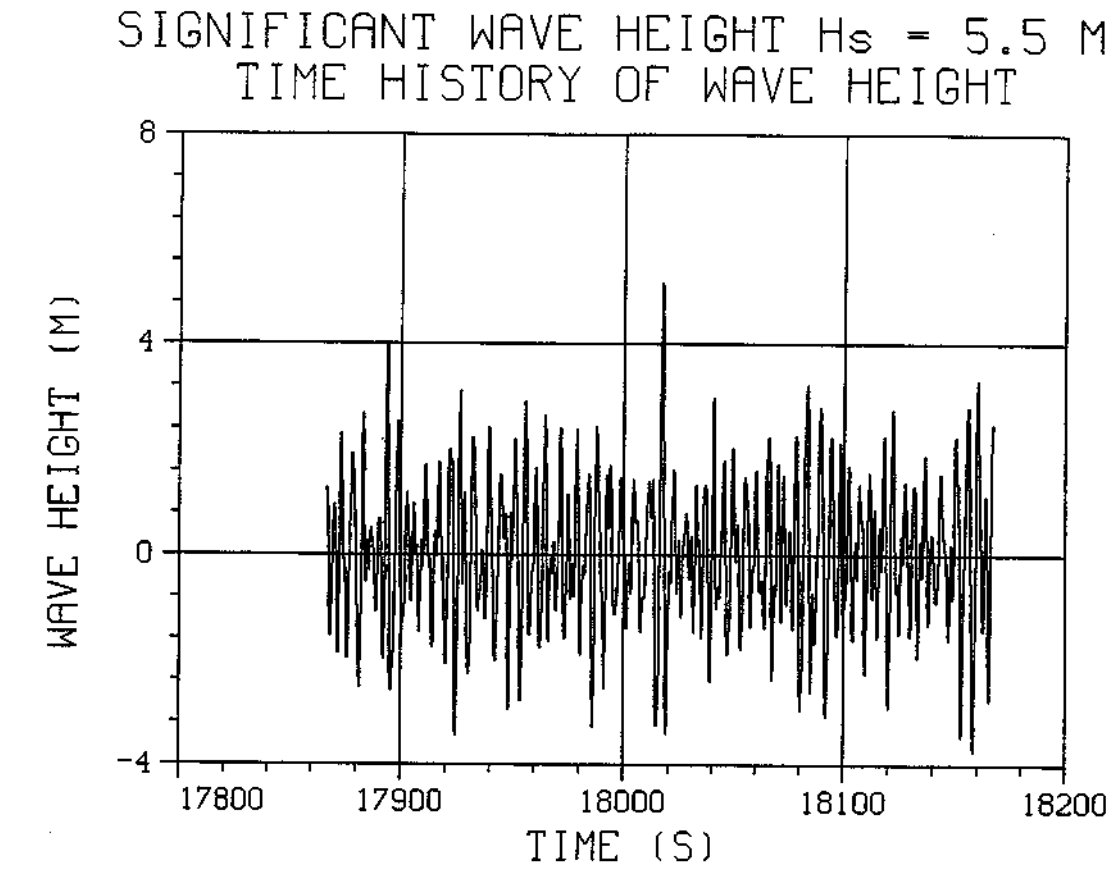

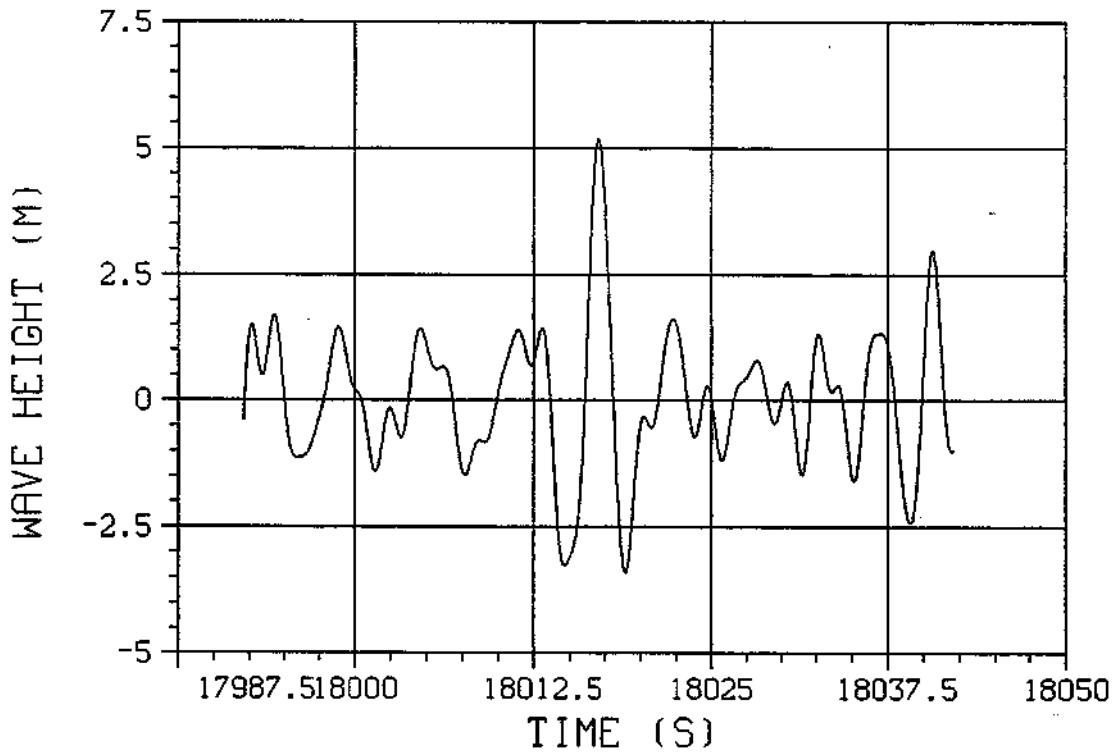

Fig. 5.1 Two short sequencies of simulated irregular waves.

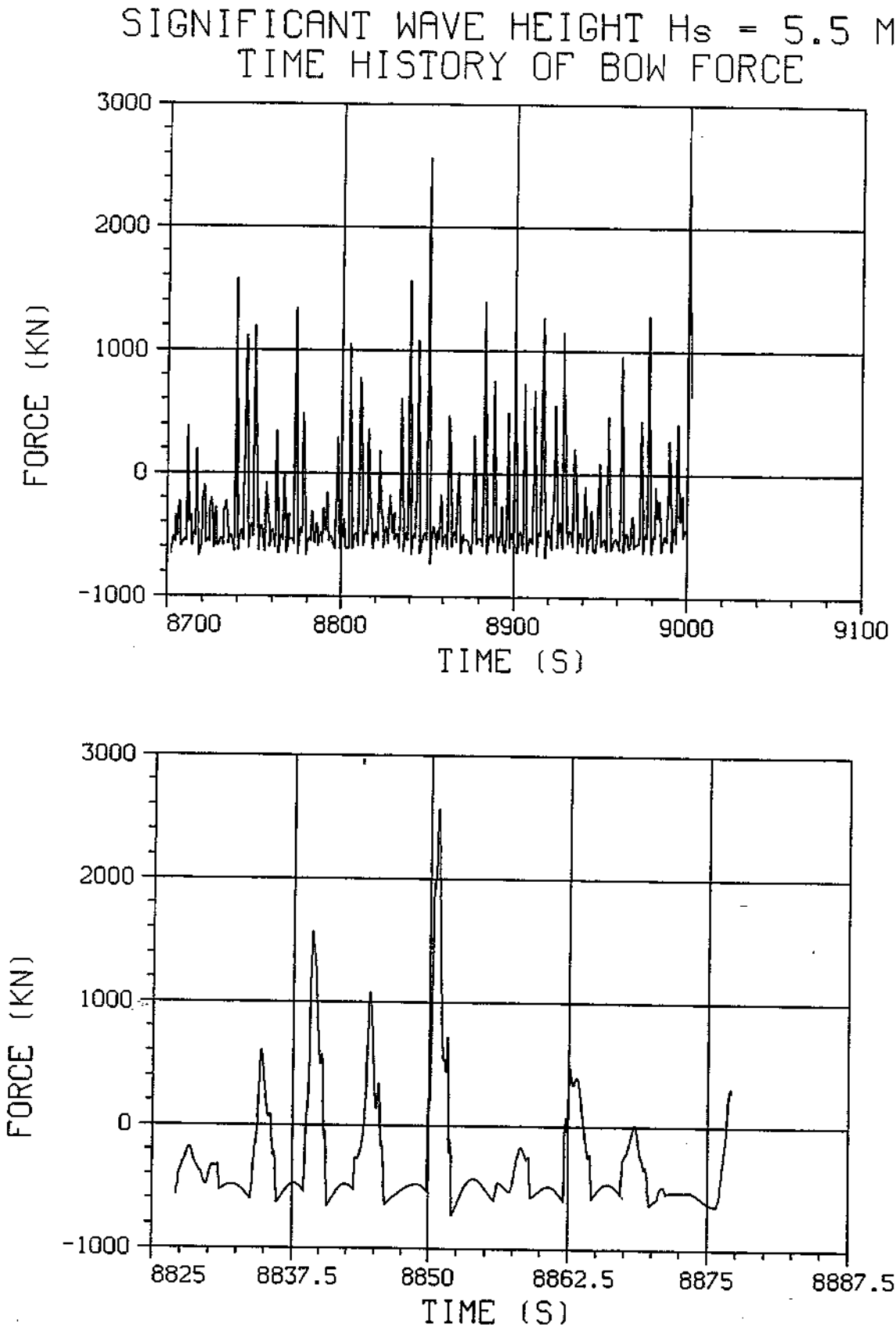

Fig. 5.2 Simulated short sequencies of vertical wave load on the visor.

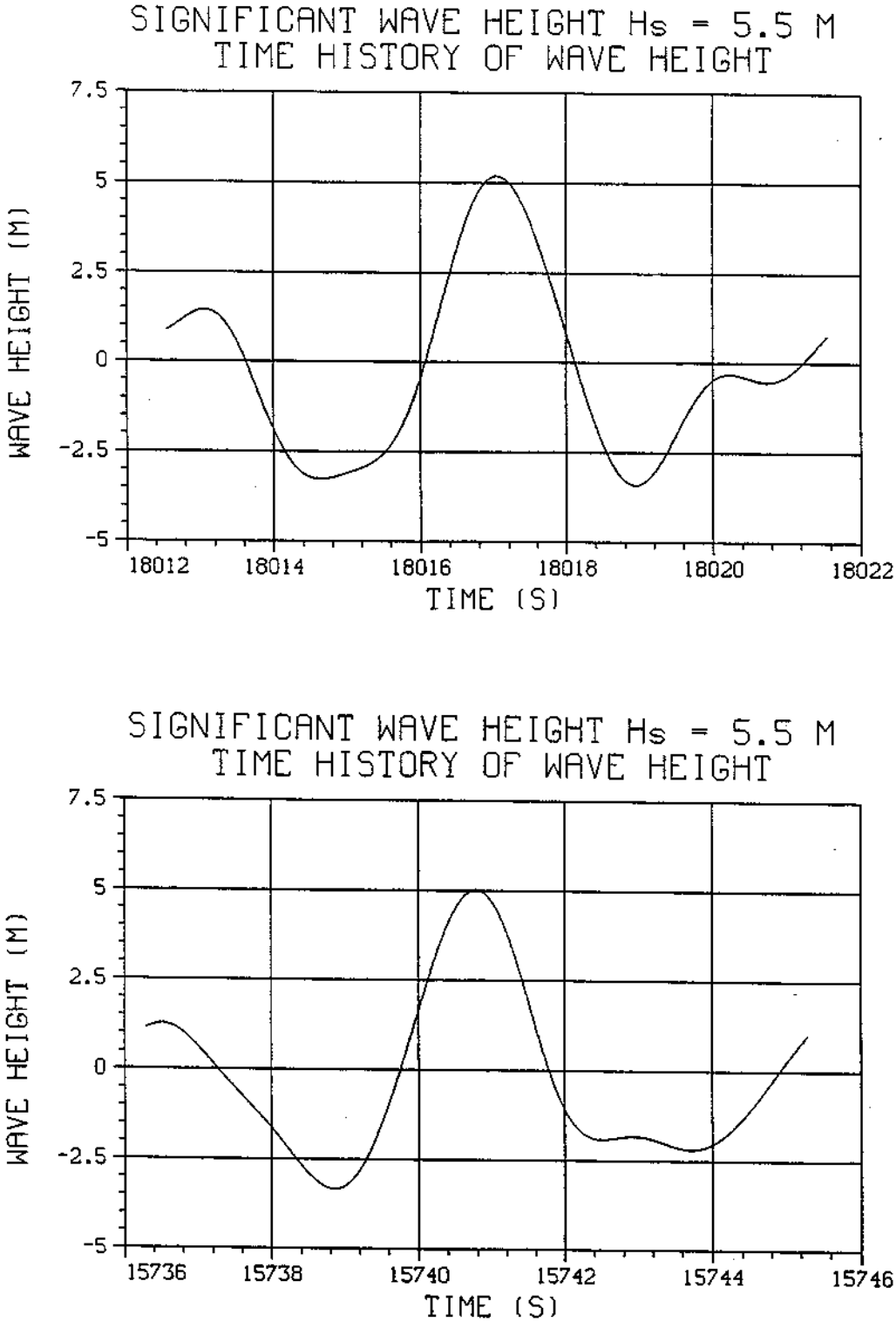

Fig. 5.3 Two high individual waves which excited significantly different loads on the visor in head seas at 15 kn speed. The wave in the upper plot excited a vertical force of 9 800 kN while the lower wave excited a force below 5 200 kN.

The amplitude of vertical relative motion at the time of the highest loads on the visor is about 6 m when the significant wave height is 4 m. A decrease in speed slightly increases the relative motion at the visor. A change of heading from head to bow seas has a similar effect on the relative motion. In the 5.5 m high waves, the relative motion amplitude associated with maximum loads is about 8 m. This means that the bow will be submerged approximately to the level of the foredeck including the bow wave height of about 1 m at 15 knots speed. The height to the foredeck from the baseline is 14.3 m. The bow submergence in the lower seastate at the time of high visor loads is about 12 m. On the basis of Figure 3.5, this is just below the draft where the volume of the visor starts to increase quickly. At a draft of 12.5 m, the visor volume is about 150 m^3 while the volume of the visor up to a draft of 15 m is about 400 m^3. Due to the strong increase of the visor area and volume upwards it may be assumed that the resultant of the wave load on the visor acts close to the water surface. Also the water particle velocities are highest on the wave surface.

In a six hours long simulation, the distribution of the load peaks has typically a long tail, i.e. a few highest peaks are significantly higher than all the other (Figures in Appendix 2). It is common that over 99 % of the peaks are smaller than half of the maximum. The distributions of wave maxima and minima (crests and troughs, respectively) in Figures A2.1 - A2.3 have a distictly different look than the load peak distribution.

Figure 5.8 shows the probability of exceedance curves for three different 36 hours simulations in bow seas at a heading of 150 degrees. The forward speed has been 15 knots and the modal period 8 s in all cases. The simulations are for the significant wave heights of 4 and 4.5 m. The effect of bow wave height has been investigated by assuming bow waves of 1 and 1.5 m heigh in the 4 m high waves. In fact, 0.33 m must be added to these nominal bow wave heights due to the actual stern trim of the vessel which has not been taken into account in predicting the bow submergence.

The significant wave height has a very strong effect on the vertical component of the visor load. The half a meter, or the 12.5 % increase in the wave height increases the wave load by over 40 %. By increasing the significant wave height from 4.0 to 5.5 m in head seas at 10 kn speed, increases the vertical loads threefoald (Figs. 5.4 and 5.6). This indicates that the loads are approximately proportional to the third power of the significant wave height. The effect of wave height is a little smaller at the higher forward speeds than at 10 knots speed. On the other hand, it seems that the highest loads roughly follow the submerged volume of the visor which is about 150 m^3 and 350 m^3 at the incidents of maximum loads when the significant wave heights are 4 and 5.5 m, respectively. In the numerical predictions, the shape of the real visor has been approximated by body which has less volume and area low down than the original one. This may have some effect on the results.

The behaviour of the bow wave in sea conditions when the vessel is heaving and pitching is not well known. The approximation of the bow wave effect at 15 knots speed by a 1.33 m high wave which is superposed on the incoming wave is a crude approximation. However, the effect of the bow wave height on the predicted forces is much less than the effect of the significant wave height. Assuming a bow wave height of 1.83 m instead of 1.33 m increases the vertical load on the visor by about 20 % when the significant wave height is 4 m or 5.5 m (Figs. 5.8 and 5.7, respectively).

Due to the larger wave-induced motions in bow seas than in direct head seas the loads on the visor are higher at 150° heading than in head waves (Figs. 5.4 and 5.8). The difference is about 20 % at the level of an 1 to 10 000 exceedance probability in 4 m high seas. An increase of the modal wave period from 8 to 8.5 s slightly increases the loads in head seas at 15 knots speed (Figs. 5.4 and 5.5).

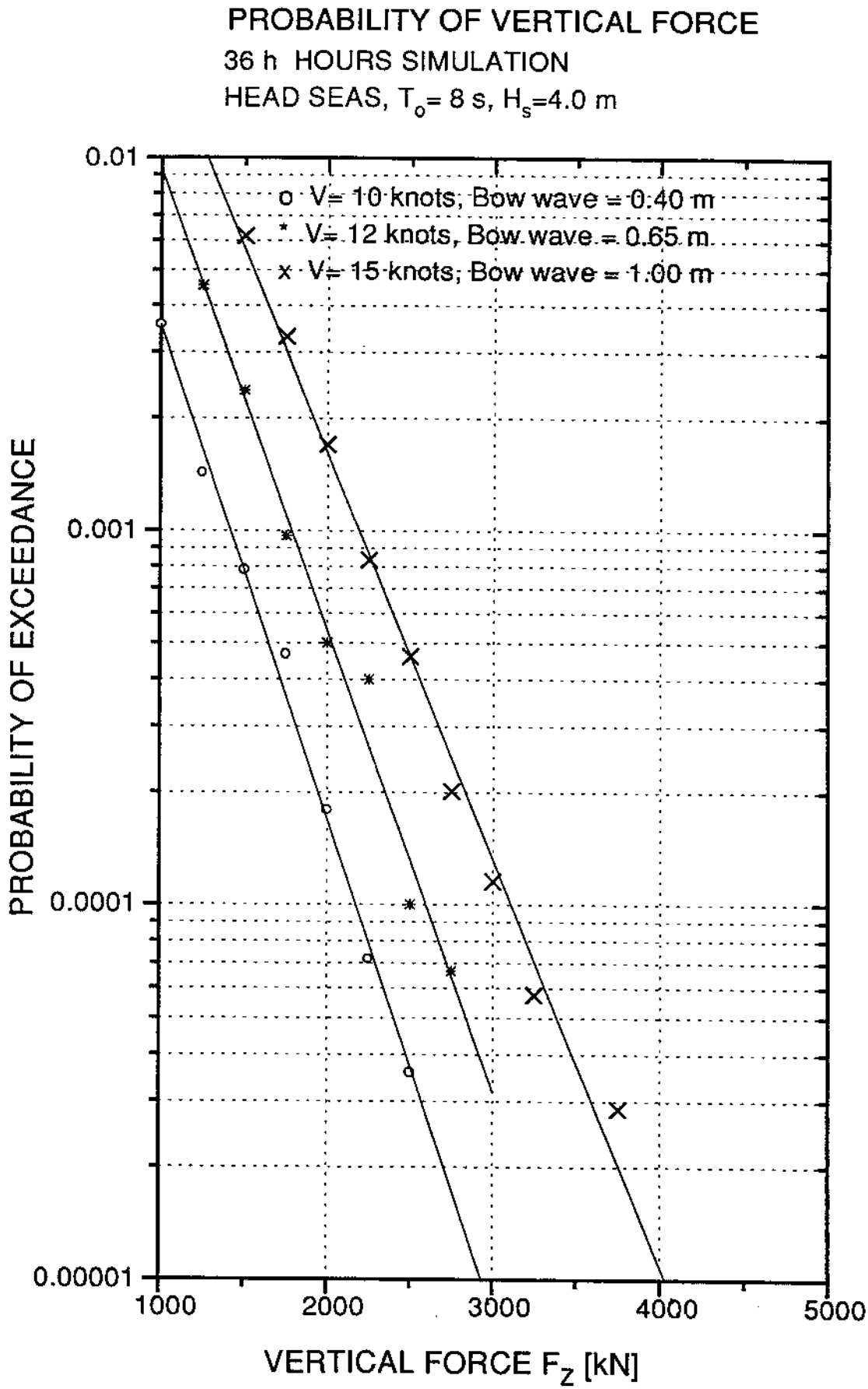

Fig. 5.4 Vertical wave loads on the visor in head seas with H_S = 4 m and T_O = 8.0 s.

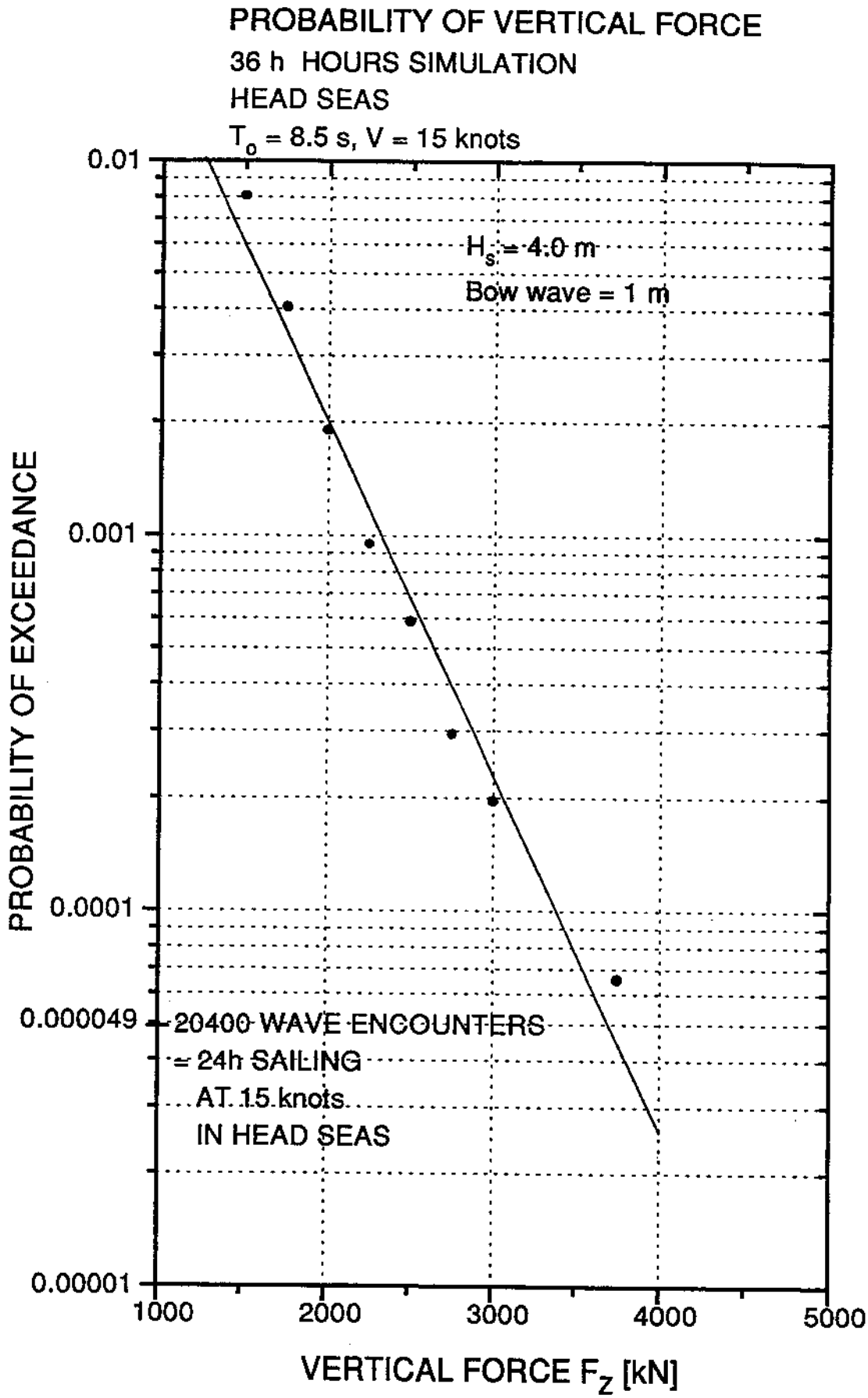

Fig. 5.5 Vertical wave loads on the visor in head seas with H_S = 4 m and T_O = 8.5 s.

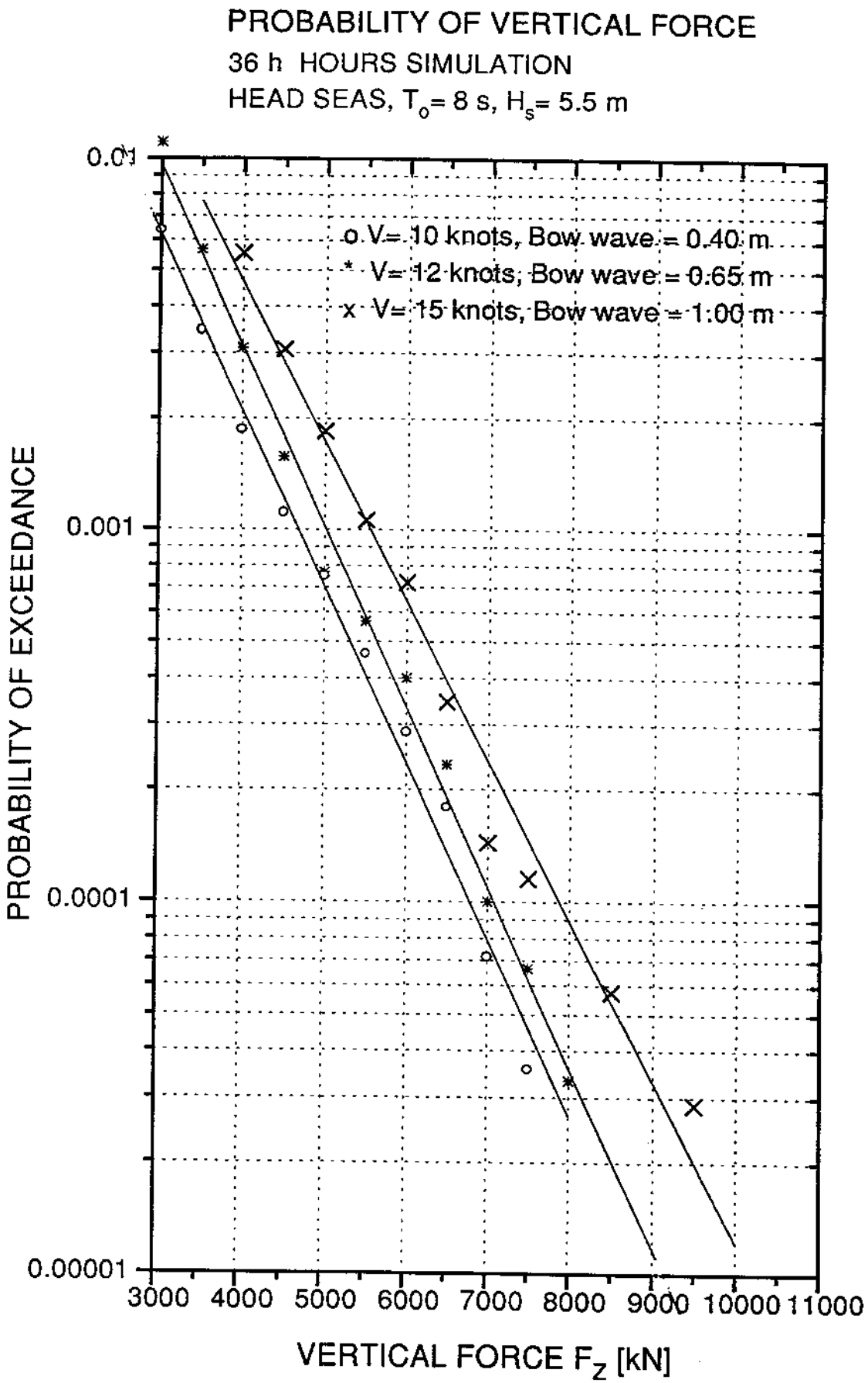

Fig. 5.6 Vertical wave loads on the visor in head seas with H_S = 5.5 m and T_O = 8.0 s.

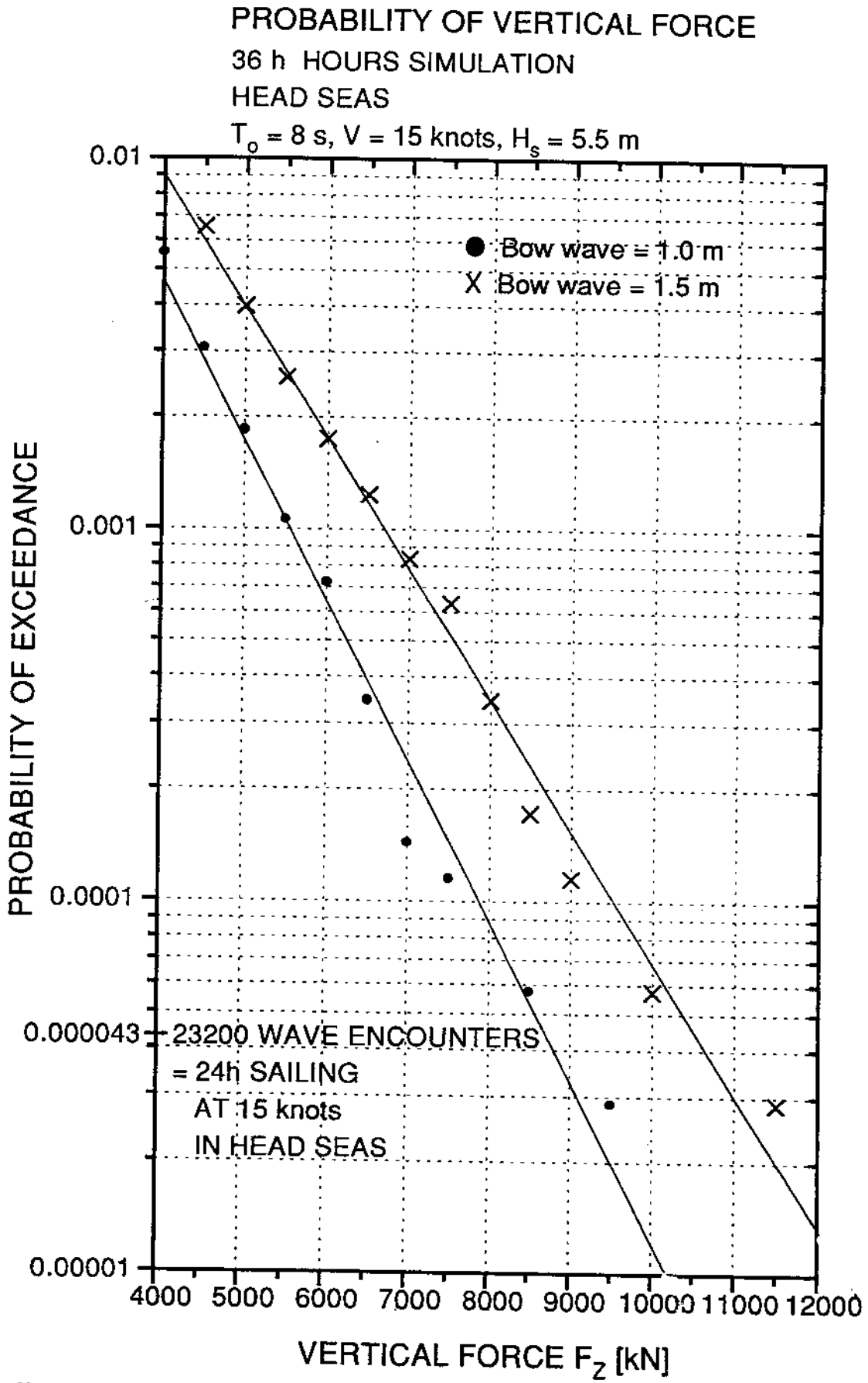

Fig. 5.7 The effect of bow wave height on the visor loads in head seas with H_s = 5.5 m at V = 15 kn.

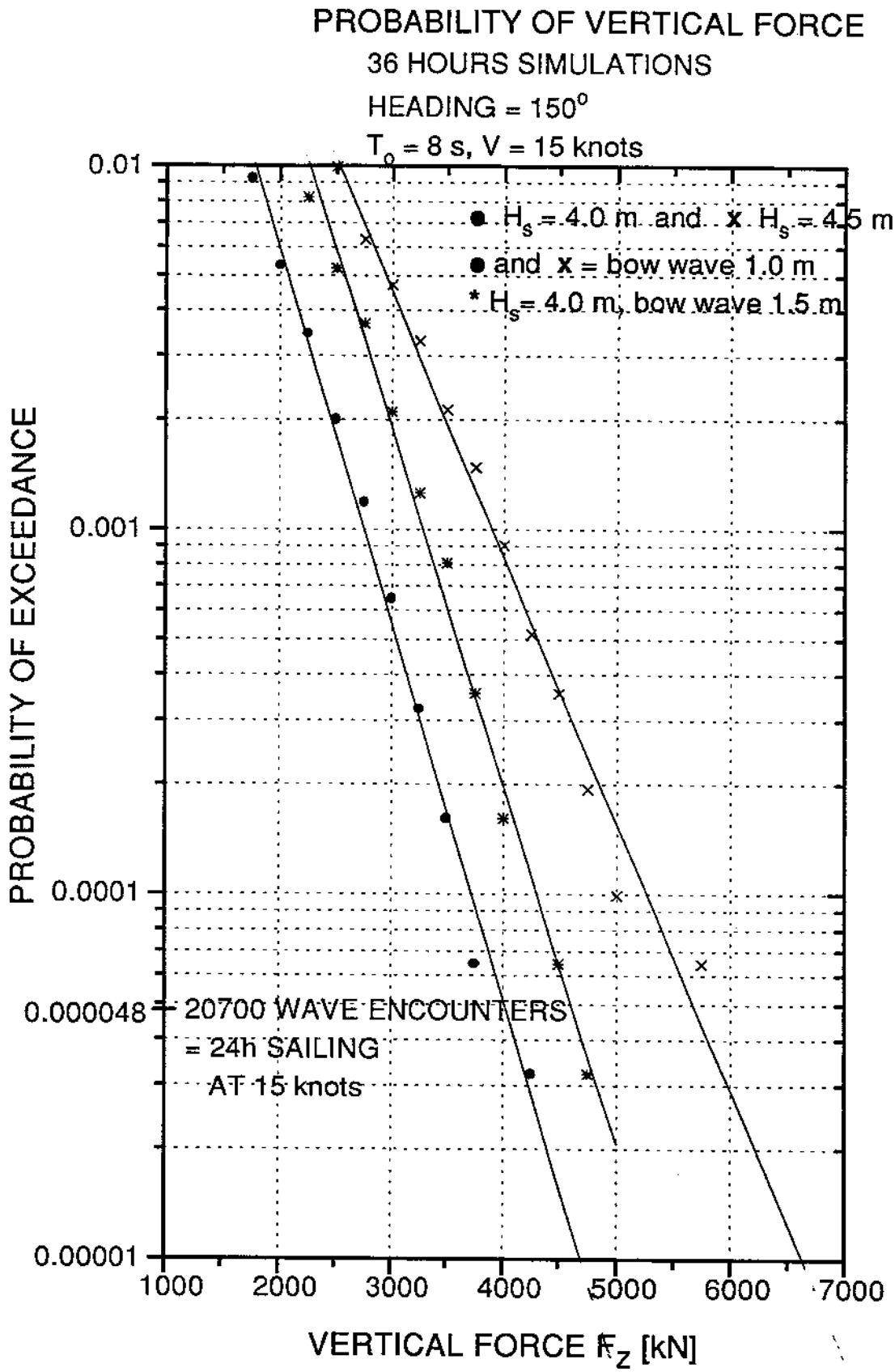

Fig. 5.8 Vertical wave loads on the visor in bow oblique seas with $H_S = 4$ m and 4.5 m.

The following table gives a summary of the vertical visor loads from different simulations.

Table 5.1 Vertical loads on the bow visor.

Heading [deg.]	Bow wave height [m]	Speed [kn]	H_S [m]	T_O [s]	Vertical visor load Exc. prob. 10^{-3}	Vertical visor load Exc. prob. 10^{-4}
Head seas, 180	1.0	15	4.0	8.0	2 200 kN	3 100 kN
Head seas	1.0	15	4.0	8.5	2 300 kN	3 400 kN
Head seas	0.65	12	4.0	8.0	1 750 kN	2 600 kN
Head seas	0.4	10	4.0	8.0	1 400 kN	2 150 kN
Head seas	0.4	10	5.5	8.0	4 700 kN	6 750 kN
Head seas	0.65	12	5.5	8.0	5 000 kN	7 100 kN
Head seas	1.0	15	5.5	8.0	5 500 kN	7 900 kN
Head seas	1.5	15	5.5	8.0	6 700 kN	9 500 kN
Bow seas, 150	1.0	15	4.0	8.0	2 750 kN	3 700 kN
Bow seas	1.0	15	4.5	8.0	3 900 kN	5 300 kN
Bow seas	1.5	15	4.0	8.0	3 400 kN	4 300 kN

Figure 5.9 summarizes the effects of forward speed and significant wave height on the visor load in head seas at the exceedance probability levels of 10^{-3} and 10^{-4}. The results in the figure show that in the lower seastate the loads increase approximately linearly with the forward speed of the vessel. At 15 knots speed, the vertical load is about 50 % larger than at 10 kn speed when the significant wave height is 4.0 m. In the higher seastate, the visor load increases by about 20 % when the speed increases from 10 to 15 knots. In this case the assumption of a 1.33 m high bow wave at 15 knots speed may be too low since the bow submerges deep down, much deeper than in the lower seastate. If a bow wave height of 1.83 m is assumed at 15 knots speed when $H_S = 5.5$ m, the wave load raises by 40 % as the speed goes up from 10 to 15 knots. The behaviour of the bow wave and its effect on the loads should be included in the numerical solution.

5.1 Comparison with the systematic model tests by SSPA

After the MV Estonia accident, SSPA has conducted an extensive, systematic series of model experiments where the wave loads on five different bow visors have been measured. The ship models represent passenger ferries which have almost equal main dimensions as MV Estonia. The main difference between MV Estonia and the SSPA ship models is that MV Estonia had V-type sections at the visor while the models of SSPA have U-type sections. In addition, the bow visor starts closer to the waterline in the SSPA models than in MV Estonia. In spite of these and some other minor differences in the hull form, it is interesting to compare the numerical predictions for MV Estonia to the experimental results of SSPA. Qualitatively the simulated and the measured records of visor loads in irregular head seas in Fig. 5.10 resemble quite a lot each other.

Figure 5.11 compares the vertical wave load on the bow visor of MV Estonia with experimental results of SSPA for the Model No. 1 in regular head waves. The wave length has been 1.2L. The predictions are for 10 and 15 knots speeds while the model tests have been carried out at speeds corresponding to 7, 10, 14 and 19 knots in full scale. The results for MV Estonia follow quite well the same trend with increasing wave height as the experimental results, but the numerical results are larger than the experimental at the same speed. At 10 knots speed, the predicted loads on the bow

visor of MV Estonia are close to the test results at 14 knots speed. A partial explanation may be that high up MV Estonia had a wider bow flare than Model No. 1 and in regular waves, close to heave and pitch resonance, the simulated motions were violent.

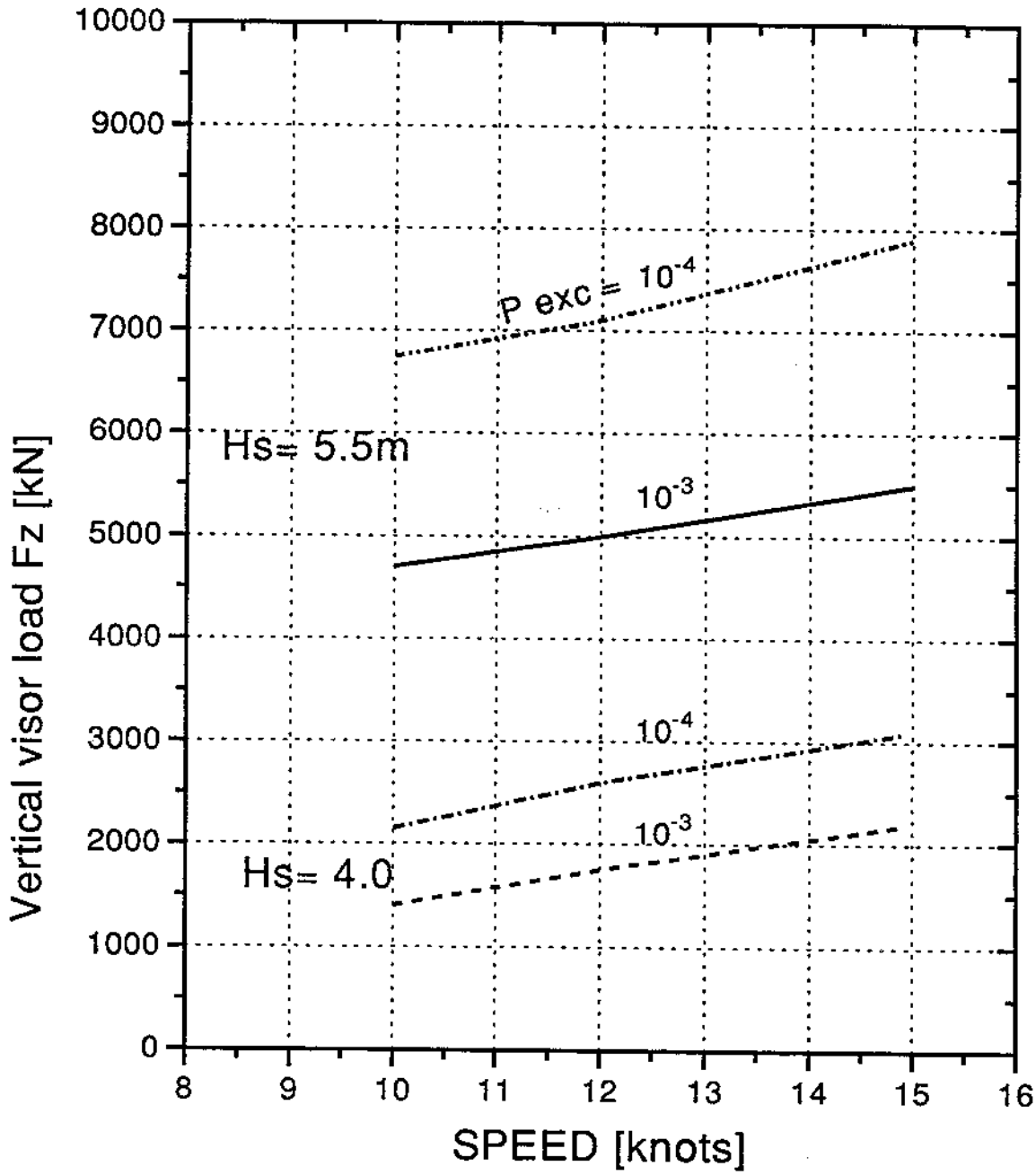

Fig. 5.9 The effect of wave height and speed on the loads of MV Estonia's visor in head seas.

SSPA MODEL EXPERIMENTS

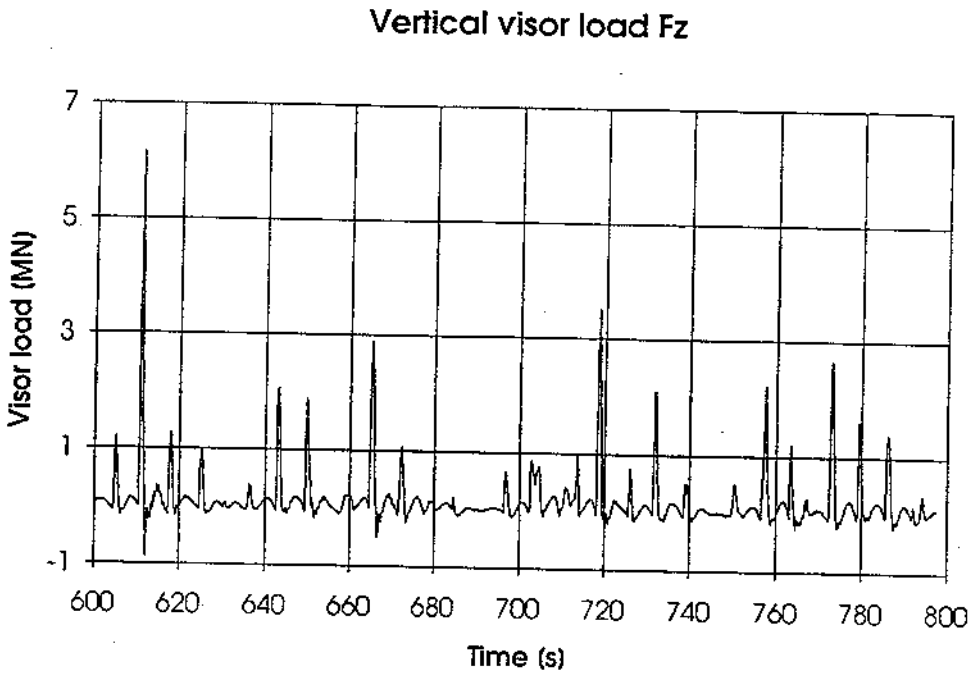

VTT SIMULATIONS

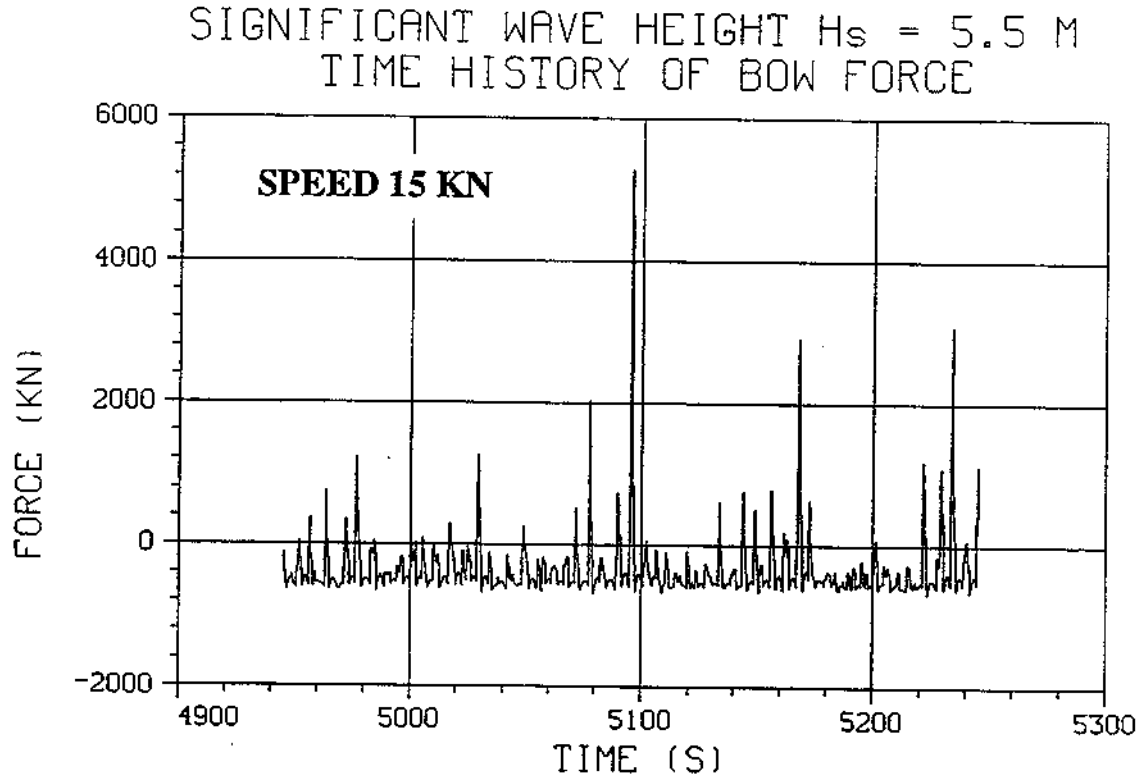

Fig. 5.10 Experimental (SSPA) and simulated records of visor loads in head seas, Hs = 5.5.

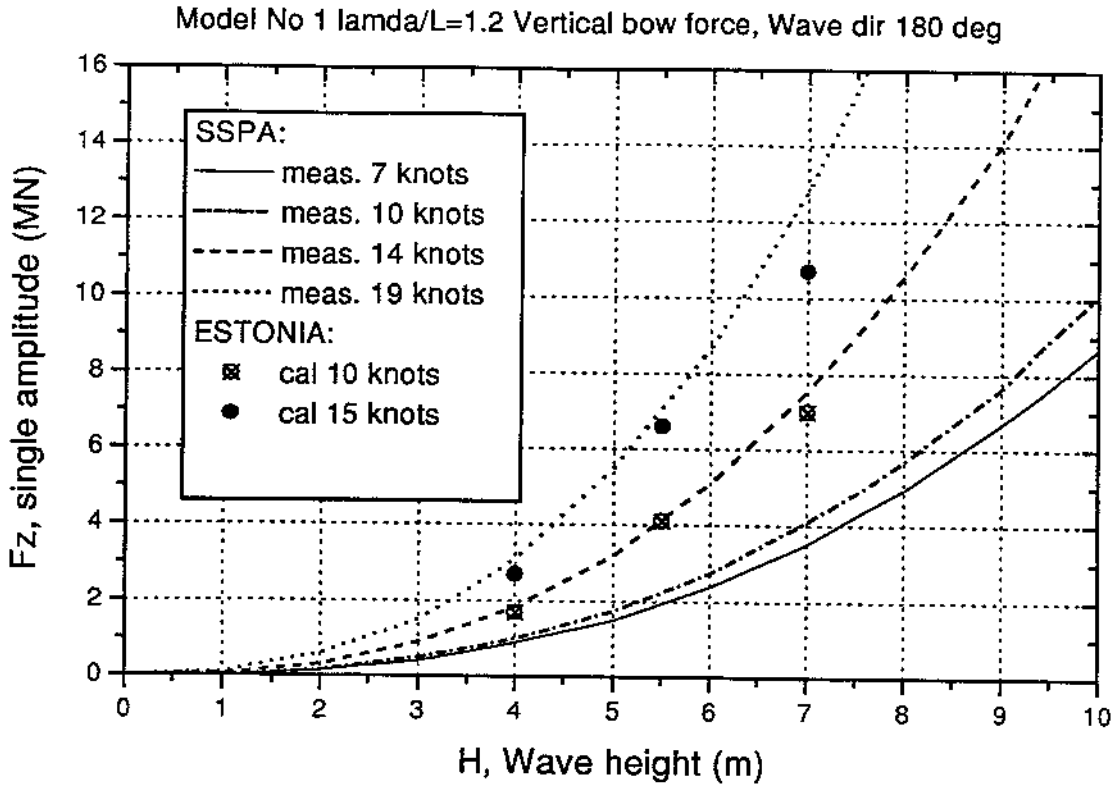

Fig. 5.11 Simulated and experimental (SSPA) vertical visor loads in regular head waves.

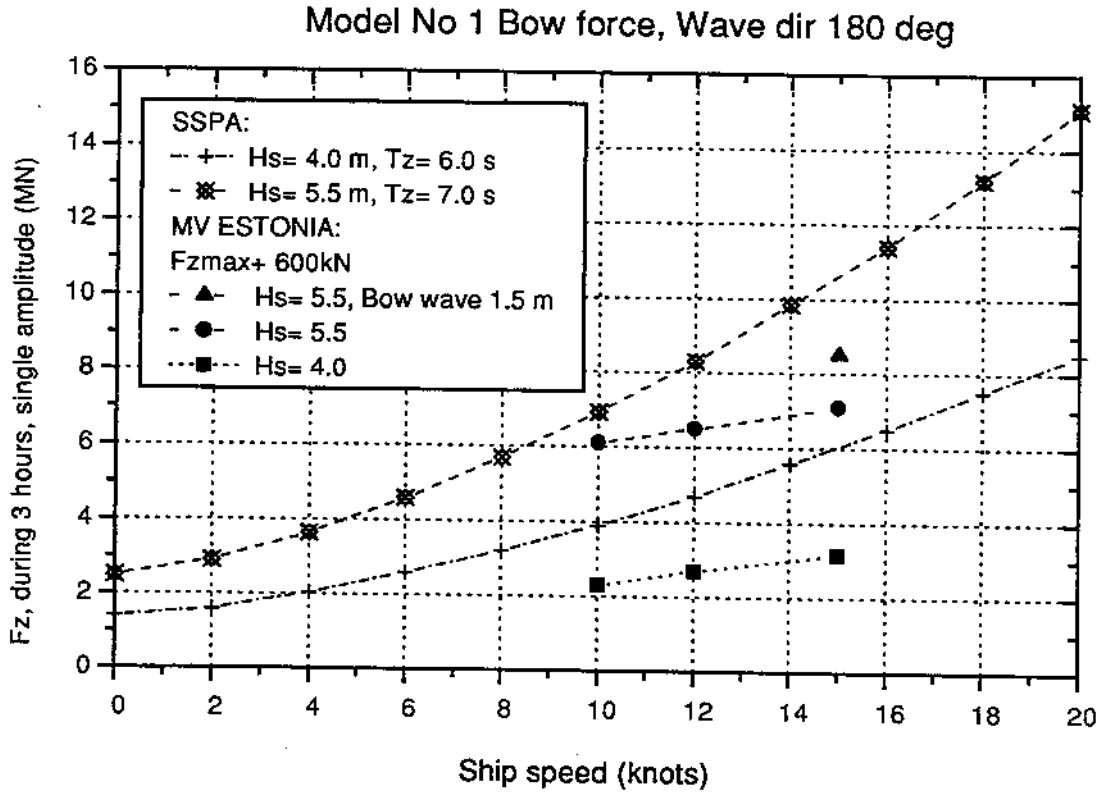

Fig. 5.12 Simulated and experimental (SSPA) vertical visor loads in irregular head seas.

In irregular head seas the simulated wave-induced motions of MV Estonia were not so violent as in high regular waves. This may have contributed to the surprising result that in irregular seas the numerical results are significantly below the model tests of SSPA. Figure 5.12 compares the results of MV Estonia to the maximum vertical visor force of Model No. 1 during 3 hours. The model test results have been extrapolated from an about one hour (full scale) long measurement to a time span of 3 hours. The results for MV Estonia correspond to the exceedance probability of 1/2 500 in Figures 5.4 and 5.6. MV Estonia encountered from 2 300 to 2 900 waves in head seas in three hours depending on the forward speed according to Table 4.2. The weight of the visor, 60 tons, has been added to the simulated results since the static situation was considered as zero level in the model tests (see Fig. 5.10).

If only the largest values measured during one hour of testing time are compared to the largest simulated values, regardless of statistics, the correlation is much better than in Fig. 5.12. This together with the comparison in regular waves (Fig. 5.11) and the strong dependence of the visor loads on the wave height suggest that the irregular wave trains in the simulations and in the model experiments may have different statistics although they have the same significant wave height. A comparison of short wave time histories representing seas with H_S = 5.5 m in the simulations and in the model experiments (Fig. 5.13) indicates that the crest heights of the experimental waves may be larger than the heights to wave troughs measured from the still water, zero level. In the experiments, minus sign indicates wave surface level above the still water surface while the opposite sign convention has been used in the simulations.

One wave record from the experiments containing about 150 waves was analysed more in detail. The peak distribution of wave single amplitudes and the level distribution are presented in Fig. 5.14. Both distributions show that the wave record includes more high crests than deep troughs. Figure 5.15 confirms that the probability of wave crest amplitude exceeding certain high level is significantly higher than the trough amplitude exceeding the same level. The exceedance probability curve of crest amplitudes differs considerably from the Rayleigh distribution which the low wave troughs follow. The simulated waves follow the Rayleigh distribution (Fig. 5.16).

Two 16 minutes long wave time histories mesured by MTL with a waverider buoy south of Bogskär in December 1982 and in January 1983 have been analysed after the MV Estonia accident to compare the wave crest and trough height distributions with the Rayleigh distribution. Figures 5.17 and 5.18 show that both the crest and trough distributions correlate well with the Rayleigh distribution. However, the wave time history measured in December 1982 contains one exceptionally high wave crest. This crest which is about 3.7 m high while the significant height is 3.3 m differs significantly from the Rayleigh distribution. In certain storm conditions, so called episodic waves which have a height of about $2.4H_s$ have been observed (Buckley, 1983), but it is not known whether this kind of waves appear in the Baltic. Andrew & Lloyd (1980) measured wave-induced motions of two British frigates in severe head seas on a full scale trial south-west of Ireland and found that the wave-induced motions follow quite well the Rayleigh distribution.

VTT SIMULATIONS

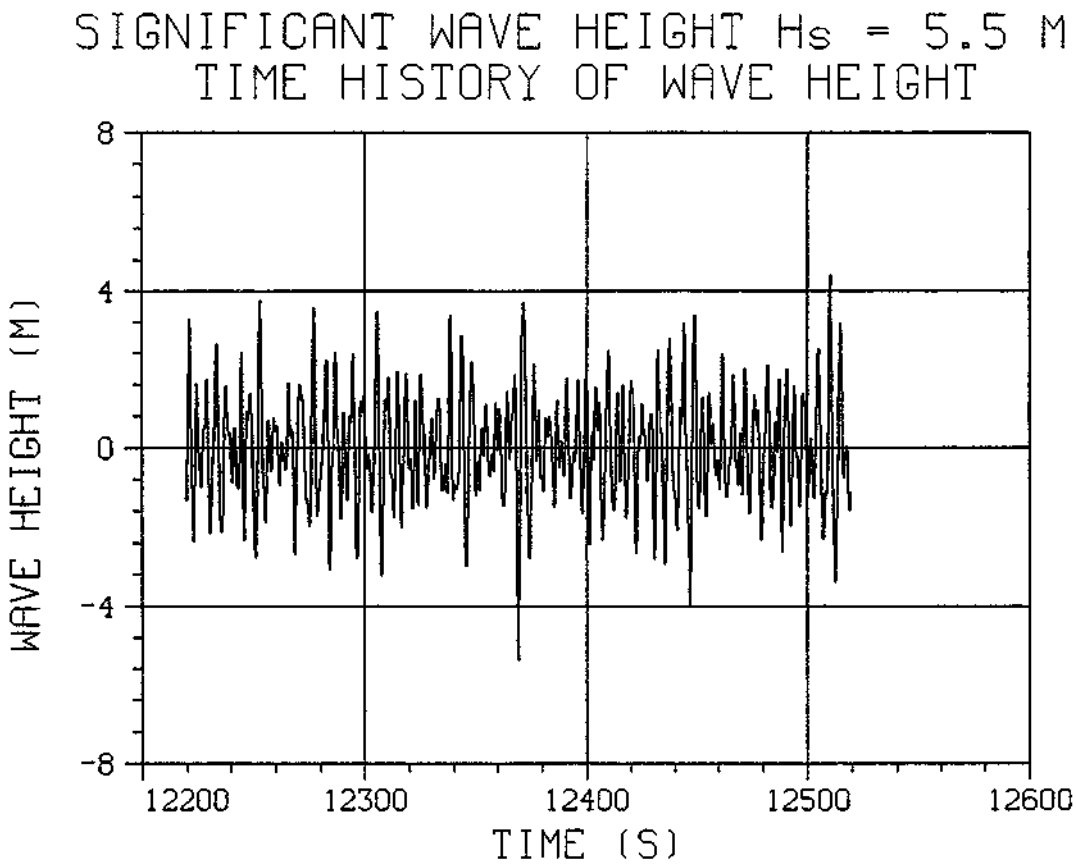

SSPA MODEL EXPERIMENTS

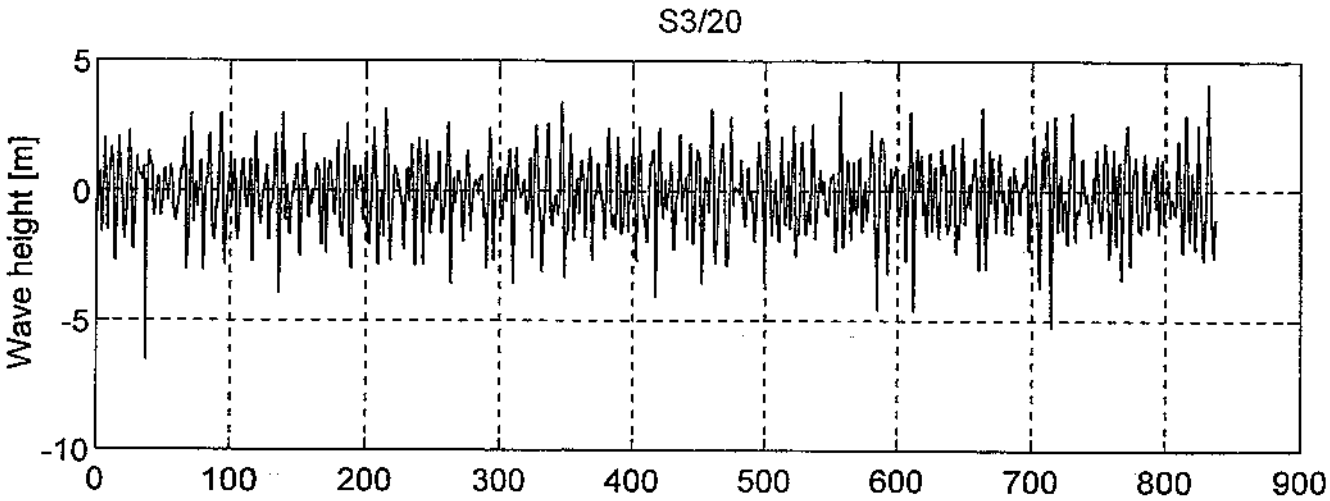

Fig. 5.13 Wave time histories from simulations and model experiments (SSPA) with H_S = 5.5 s.

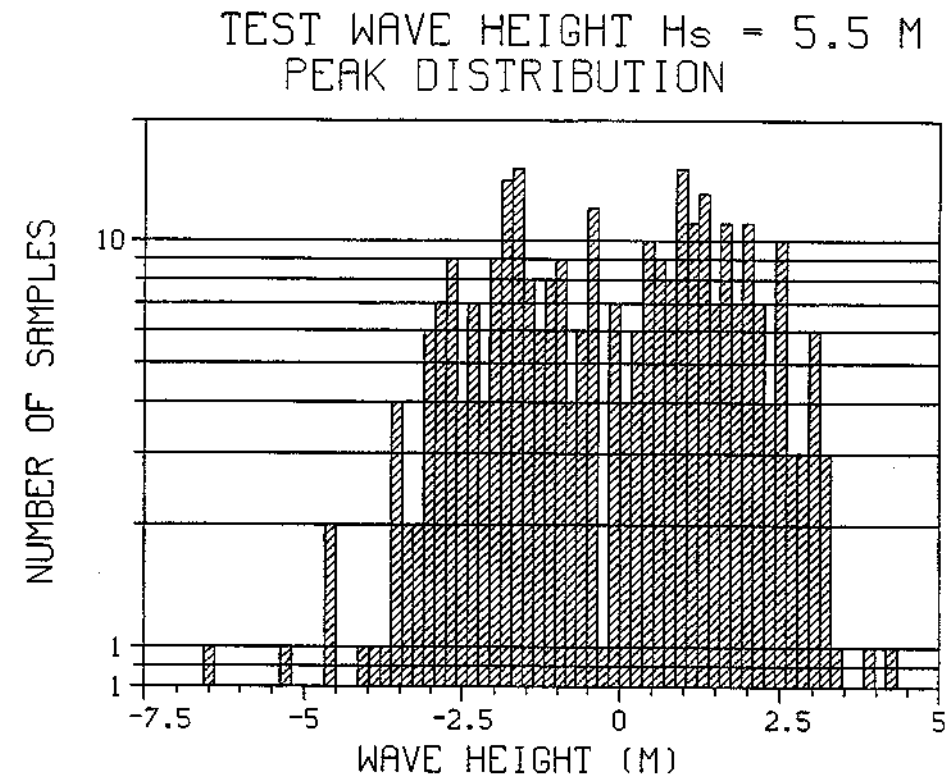

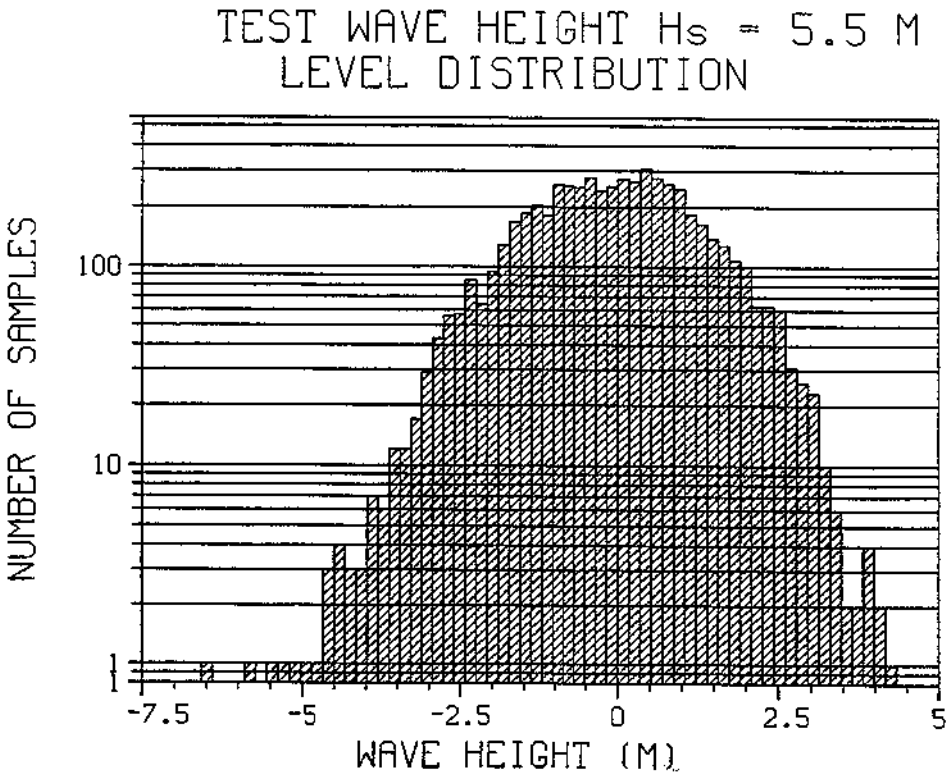

Fig. 5.14 Peak and level distributions of a wave record from the model tests by SSPA.

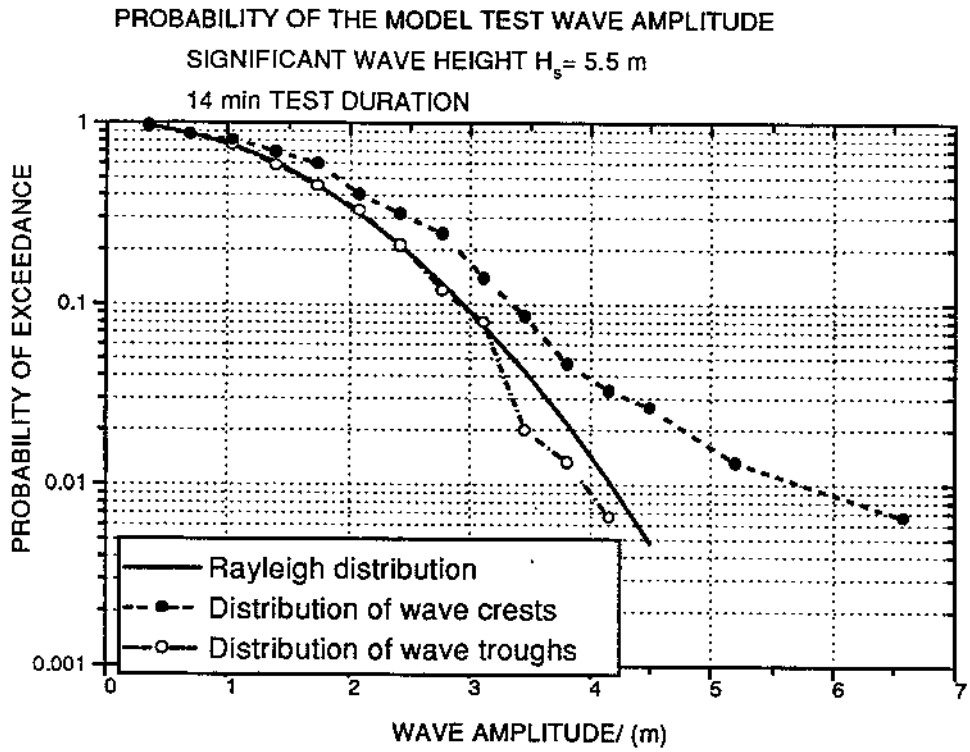

Fig. 5.15 Exceedance probabilities of wave crest and trough amplitudes from model tests by SSPA compared to the Rayleigh distribution.

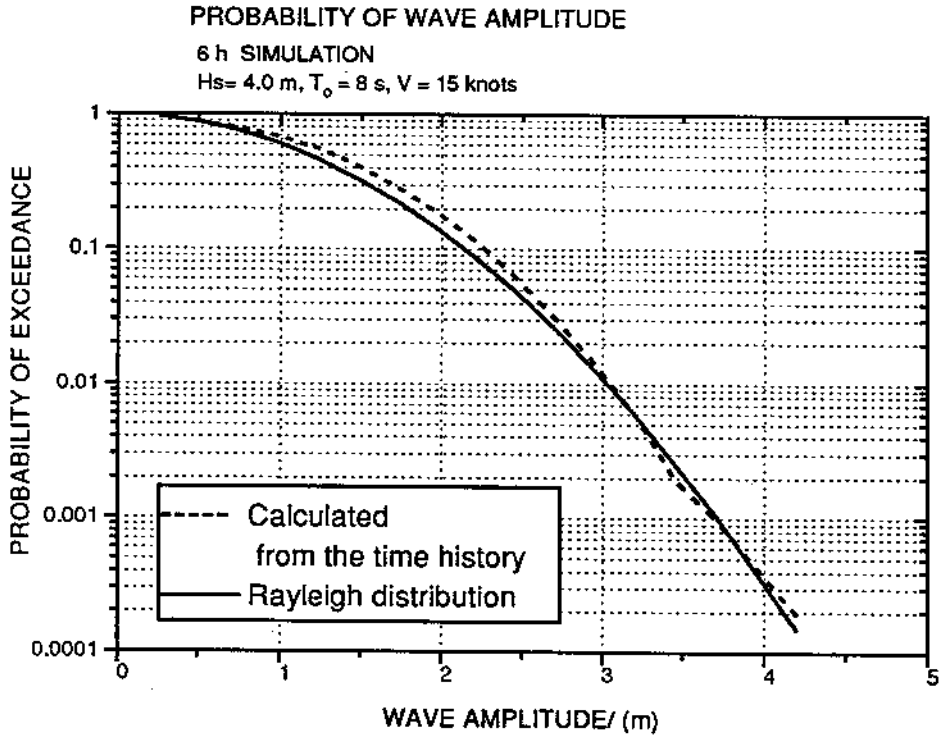

Fig. 5.16 Exceedance probabilities of wave amplitudes of a simulated wave record compared to the Rayleigh distribution.

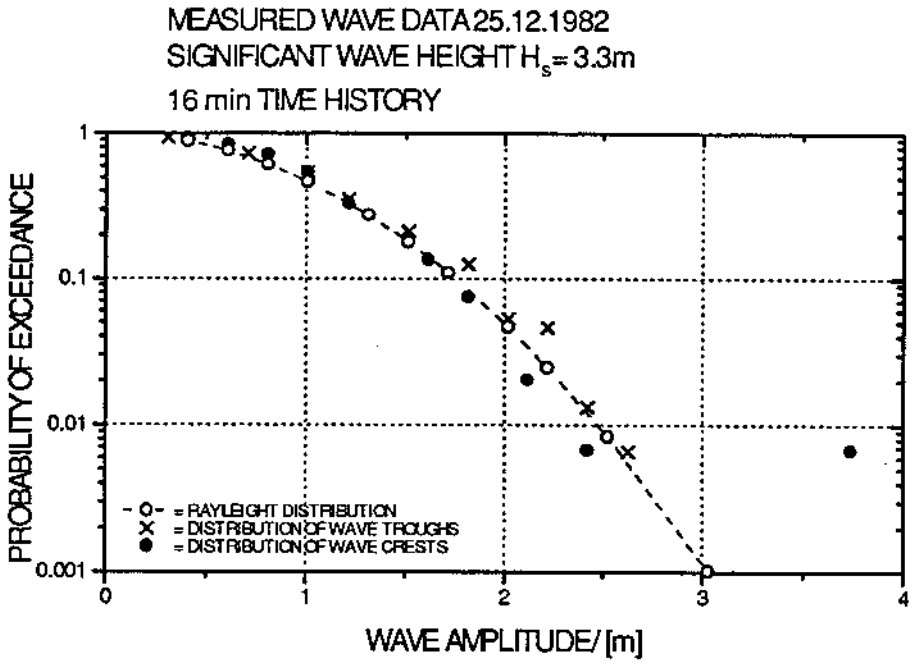

Fig. 5.17 Distribution of wave crest and trough amplitudes measured in December 1982 south of Bogskär compared to the Rayleigh distribution.

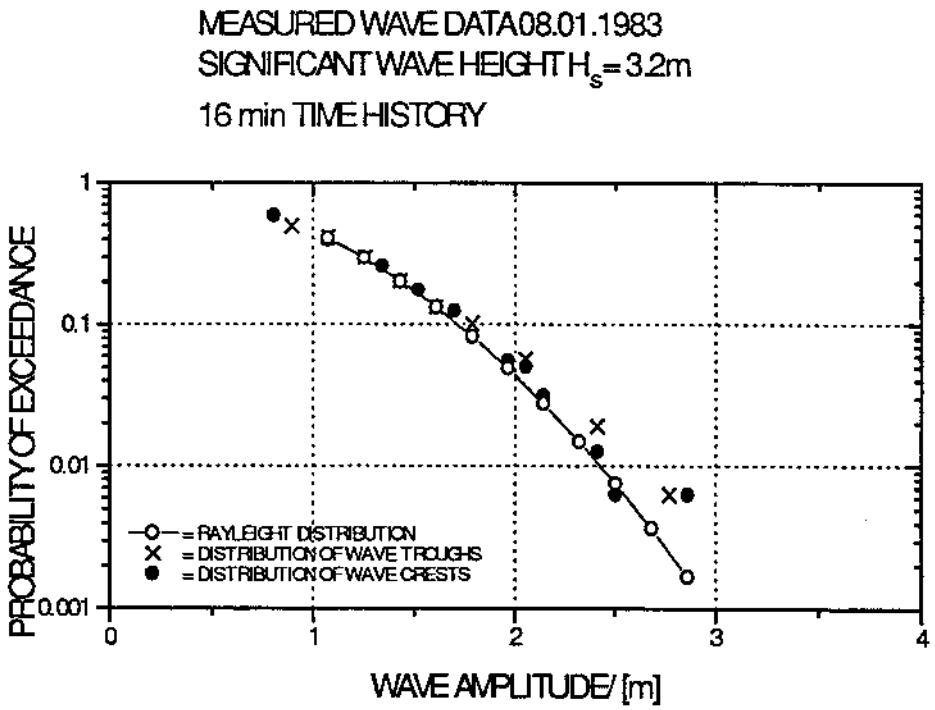

Fig. 5.18 Distribution of wave crest and trough amplitudes measured south of Bogskär in January 1983 compared to the Rayleigh distribution.

5.2 Comparison with experiments with the model of MV Estonia

Model tests with a model of MV Estonia have been carried out by SSPA to measure the wave-induced loads on the bow visor. The tests and the results have been reported in the SSPA Report 7524 dated 1995-12-05 and in the Appendix to the report. The test program included runs in regular and irregular head and bow waves at speeds 10, 15 and 19 knots. The significant wave heights used with JONSWAP spectra were 4, 4.5 and 5.5 m.

The maximum measured vertical force component on the visor has been compared to the simulated vertical force having a probability of exceedance corresponding to the measurement time in the model experiments. The following table shows the relevant experimental results in irregular seas and the simulated results corresponding to the test conditions which are also given in the table.

Table 5.2 A comparison of simulated and experimental vertical wave loads on the visor.

SSPA runs	Head.	V [kn]	H_s [m]	Measur. time [s]	Wave enc. VTT	F_z max. meas. SSPA	F_z est. meas. SSPA	F_z sim. VTT
4-5	Head	10.0	3.787	1 922	414	1.817 MN	1.8 MN	1.7 MN
6-31	Head	15.0	3.945	19 161	5 145	6.214 MN	6.2 MN	3.5 MN
34,35,42	Head	10.0	5.233	3 582	771	6.265 MN	5.4 MN	5.0 MN
36,37,41	Head	15.0	5.367	2 345	630	5.939 MN	5.9 MN	5.6 MN
7-13	Head	14.86	4.096	1 649	443	4.980 MN	2.9 MN	2.4 MN
67-116	Bow	14.54	4.512	10 672	2 557	7.400 MN	5.9 MN	5.1 MN

Table 5.2 gives the run numbers specified in the SSPA report, measured average forward speed, V, and significant wave height, H_s, total measurement time, and the number of wave encounters in the VTT simulations corresponding to the measurement time. F_z max. is the maximum vertical force component on the visor measured during the experiments at the particular speed, heading and significant wave height. In the SSPA report, the given force is defined as the nominal force since it has been corrected for the difference in mass of the model visor and the full scale visor. However, the weight of the visor has not been included in the vertical force. Thus, the weight of the visor, 0.6 MN, has been added to the simulated forces given in the table.

The simulated forces F_z sim. have been estimated from the probability of exceedance curves in Figures 5.4, 5.6 and 5.8. The forces correspond to the exceedance probabilities of 1/(number of wave encounters), for instance, in bow seas at 14.5 kn speed the exceedance probability has been 1/2 557 = 0.00039. If the maximum force measured during the experiments differs considerably from the general trend of the lower peak force values expressed in the form of a Weibulll-diagram, the general trend has been extrapolated and an estimate F_z est. has been read from the extrapolation line. This has been made in three cases of which examples are in Figure 5.19.

As expected, the simulated vertical forces are smaller than the measured forces. The difference cannot be explained by viscous effects which are of the order of 0.01 MN. Also the computed significant relative motions and velocities agree well with the measured data (Report VTT VALC53) so that a discrepancy in the simulated and experimental wave-induced motions seems to be not a source of the difference. The correlation of the numerical predictions is better with the estimated experimental value than with the measured maximum value. However, if the maximum measured value follows the general trend, the correlation with the numerical prediction is quite good with the exception of the head sea case at 15 kn, runs 6 - 31, H_s = 3.945 m. For instance, at 15 kn speed in

head seas with a significant height of 5.367 m the maximum measured value is 5.9 MN while the corresponding force from the simulations is 5.6 MN.

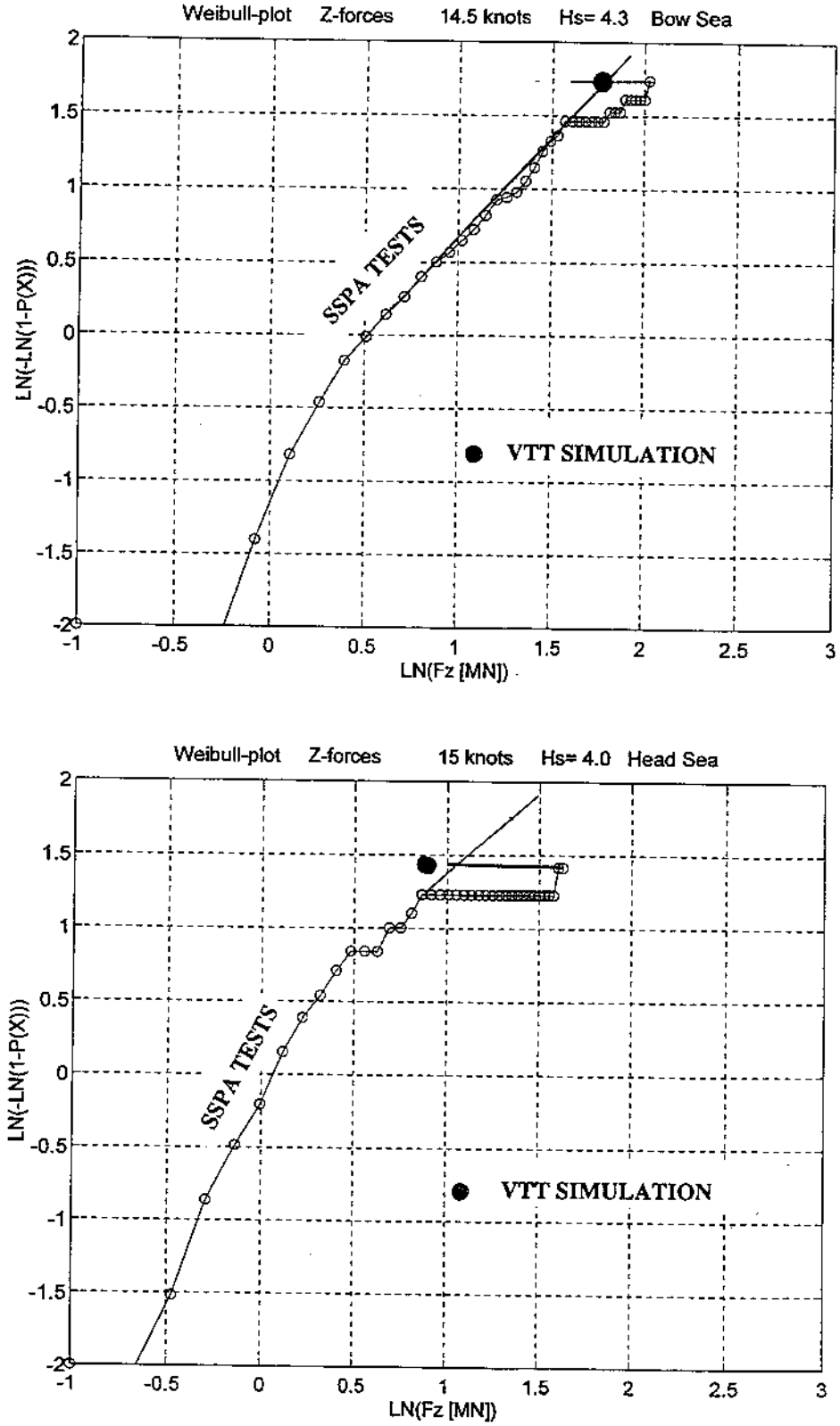

Figure 5.19 Extrapolation of measured data and a comparison with simulated results.

The maximum vertical force measured during the runs 6 - 31 in the towing tank at 15 kn speed, 6.2 MN, is significantly higher than the simulated value of 3.5 MN although the maximum follows quite well the general trend of the lower measured peak values. A partial explanation may be that the wave time histories in runs 6 - 31 have included some quite extreme wave crests and the distribution of high wave crest amplitudes differs considerably from the Rayleigh distribution like in Figure 5.15. The maximum measured wave crest amplitude has been 7.012 m which is rather extreme when the significant wave height is 3.945 m. It must be noted that the highest forces are not excited by the highest wave crests, for instance, during the runs 6 - 31 the maximum force is due to a 5.3 m high crest. However, it may be anticipated that if the wave crest heights are extreme also those wave characteristics which are significant for high loads on the visor may be extreme.

To understand better the correlation of high visor loads with ship motions and characteristics of waves, Table 5.3 below shows a summary of experimental wave and response maximum values.

Table 5.3 Experimental wave and response maximum values.

SSPA runs	Head.	V [kn]	H_s [m]	H max [m]	H crest max. [m]	Rel. mot. max. bow down [m]	Rel. vel. max. bow down [m]	F_z max. meas. SSPA
4-5	Head	10.0	3.787	6.33	4.197	5.69	6.77	1.817 MN
6-31	Head	15.0	3.945	8.19	7.012	7.60	10.65	6.214 MN
34,35,42	Head	10.0	5.233	9.55	7.056	7.41	9.22	6.265 MN
36,37,41	Head	15.0	5.367	9.07	6.587	6.94	12.09	5.939 MN
7-13	Head	14.86	4.096	8.84	6.145	7.41	7.22	4.980 MN
67-116	Bow	14.54	4.512	8.40	5.894	7.59	10.94	7.400 MN

Table 5.3 indicates that the maximum vertical force correlates better with the maximum crest amplitude measured upwards from the calm water level than with the maximum relative motion or velocity amplitude in the bow down motion. The correlation with crest height is also better than with the maximum crest-to-trough wave height, H max. Though the observed correlation may be just a chance, the ratios of the maximum measured vertical force to the square of maximum crest amplitude are given in the following table.

Table 5.4 Experimental ratio of the maximum force to maximum crest height squared.

SSPA runs	Head.	V [kn]	H_s [m]	H max. [m]	H crest max. [m]	F_z max. meas. SSPA	$F_z$max./ (H crest)^2
4-5	Head	10.0	3.787	6.33	4.197	1.817 MN	0.103
6-31	Head	15.0	3.945	8.19	7.012	6.214 MN	0.126
32-33	Head	19.0	4.036	7.29	5.418	8.523 MN	0.290
34,35,42	Head	10.0	5.233	9.55	7.056	6.265 MN	0.126
36,37,41	Head	15.0	5.367	9.07	6.587	5.939 MN	0.137
38-40	Head	19.0	5.289	9.55	7.260	8.148 MN	0.155
7-13	Head	14.86	4.096	8.84	6.145	4.980 MN	0.132
34-46	Bow	9.86	4.207	8.08	5.084	2.373 MN	0.092
67-116	Bow	14.54	4.512	8.40	5.894	7.400 MN	0.213
48-55	Bow	10.0	5.338	9.55	6.189	7.318 MN	0.191
56-66	Bow	15.1	5.286	10.05	6.914	10.846 MN	0.227

It is once again stressed that the maximum wave crest given in Table 5.4 did not cause the maximum vertical force given in the same table though there seems to be some correlation between them. The

table seems to indicate that speed has some effect on the vertical visor load, i.e. the ratio of the force to the crest height squared increases with increasing speed. A change of heading from head to bow seas increases clearly the force ratio. Respectively, the wave-induced motions are clearly larger in bow seas than in the head seas while a speed increase has a modest effect on the motions as the results in the report VTT VALC53 show. It is surprising to see in Table 5.4 that in head seas at 19 kn speed a larger maximum force has been measured in the seastate with H_s = 4.036 m than in the seastate with H_s = 5.289 m. The explanation may be statistics since in the lower seastate the maximum force differs very significantly from the Weibull fit through the lower values. If a value corresponding to the measured maximum is read on the extrapolation line, a vertical force of about 4.5 MN is obtained. This force divided by the square of crest height gives 0.153 which is very well in line with the other values.

5.3 Wave loads on the bow visor of MV Estonia during the last voyage

During the last voyage of MV Estonia, the significant wave height rose to near 4 m about one hour before the accident, or at about midnight Finnish time. During this one hour, the vessel encountered about 1 000 waves. Thus, it is quite likely that the maximum vertical load exceeded the value corresponding to the exceedance probability of 1/1000. There is a chance of 1 to 10 that during one hour the extreme load was larger than the value corresponding to the exceedance probability of 1/10 000. The extreme load increases by about 1 000 kN with a decrease of the exceedance probability from 10^{-3} to 10^{-4}.

Due to the approximations involved in the numerical method, it is believed that the extreme load values may be larger in reality than the simulated values. The simplified form of the visor acts in this direction in lower seas and the lack of non-linear, breaking waves in the simulated wave time histories has a similar effect. Due to the wind shift south the seas may have been short-crested and quite confused which increases wave-induced motions and wave loads on the visor. Taking this into account it seems quite well possible that MV Estonia hit in bow seas at a speed of 15 knots a wave which generated on the visor a vertical load exceeding 5 000 kN, even 6 000 kN at a somewhat smaller exceedance probability. The numerical predictions show an approximately linear relationship between the vertical visor load and the forward speed of the vessel.

The numerical predictions give only the vertical component of the wave load on the visor. To determine also the visor opening moment around the hinges, the horizontal force component, the point of application and the direction of the total force have to be estimated. The predictions by the SHIPFLOW-program and the shape of the visor suggest that the horizontal load component is approximately equal to the vertical component which has been confirmed by the model experiments. It seems reasonable to assume that the acting point of the total load has been at or somewhat below the vertical centre of buoyancy of the submerged part of the visor close to the stem. The total force has thus been acting at a height of about 11.5 m above the baseline, or 6 m above the design waterline of T = 5.5 m. On the basis of the visor geometry, the force resultant has been acting in a direction which is nearly perpendicular to the stem. These assumptions result in a moment arm of about 3 m and a total opening moment around the hinges of over 20 MNm.

The significant wave height has a strong effect on the bow flare loads as already noted by Gran et al. (1976). According to the Finnish Institute of Marine Research the uncertainty in the estimate of the significant wave height is about 0.5 m. The numerical predictions indicate that a change of H_s by 0.5 m may change the vertical load on the bow visor of MV Estonia by 1000 to 1 500 kN. In head seas with H_s = 5.5 m at a speed of 15 kn, the vertical visor load may exceed 10 000 kN.

5 CONCLUSIONS

The vertical component of the wave load on the bow visor of MV Estonia has been simulated in irregular head and bow seas by a numerical method based on the so called non-linear strip method and momentum consideration. The method is practical and seems to give reasonable results in spite of the simplifying assumptions involved in the method. The simplifications probably decrease the numerical visor load values. This has been taken into account before making the final load estimates. The method has not been fully validated but in some cases the results for MV Estonia have been compared with results of model tests with some other hull forms and with a model of MV Estonia. The comparison of numerical predictions with experimental results of MV Estonia is encouraging though the different factors contributing to high visor loads are not clear.

The numerical predictions indicate that the vertical component of the wave load on the bow visor of MV Estonia may quite well have exceeded 5 000 kN or even 6 000 kN at a somewhat smaller probability in the sea conditions of the accident night. The results of the numerical predictions supplemented by some rough estimates of the direction and acting point of the load resultant suggest a visor opening moment around the hinges of over 20 MNm.

The very strong dependence of the visor loads on the wave height and even on the wave shape adds uncertainty in the results. This dependence arises partly from the wide flare of the bow visor of MV Estonia. The dependence of the vertical visor load on the forward speed of the vessel is not nearly so strong as on the significant wave height. The load on the bow visor of MV Estonia seems to be approximately directly proportional to the forward speed over a speed range relevant on the accident night.

The behaviour of the "steady" bow wave when the bow submerges deeply is not well known. In the numerical predictions, the bow wave height estimated by a non-linear numerical method in calm water has simply been superposed to the vertical relative motion at bow. Assuming a higher bow wave increases the loads. The behaviour of the bow wave should be part of the numerical solution.

The irregular seas used in the simulation have been generated by applying the linear superposition principle. This means that the wave crests and troughs are symmetrical with respect to the still water level and the crest and trough amplitudes follow the Rayleigh distribution. In reality in rough sea conditions, the wave troughs get flatter and the wave crests sharper resulting finally to wave breaking. This increases the number of high wave crest amplitudes and decreases the number of deep throughs. The result is evidently an increase in the magnitude and probability of high wave loads on the bow visor. Wave groups of successive high waves act also in this direction by inducing large motion displacements to the vessel. These are problems which require further study.

VTT VALMISTUSTEKNIIKKA
Laiva- ja konetekniikka
VTT MANUFACTURING TECHNOLOGY
Maritime Technology
P.O. Box 1705
FIN-02044 VTT
FINLAND
Tel.int.+358 0 4561
Telefax +358 0 455 0619
Telex 122972 vttha sf

REFERENCES

Buckley, W. H. 1983. A study of extreme waves and their effects on ship structure. Ship Structure Committee Report SSC-320, U.S. Coast Guard, Washington, D. C. 82 p.

Chiu, F. & Fujino, M. 1991. Nonlinear prediction of vertical motions of a fishing vessel in head sea. Journal of Ship Research, Vol. 35, No. 1, March, pp. 32 - 39.

Faltinsen, O. M. 1990. Sea loads on ships and offshore structures. Cambridge University Press, Great Britain, 328 p.

Garrison, C. J. 1974. Hydrodynamics of large objects in the sea. Journal of Hydronautics, Vol. 8, No. 1, January, pp. 5 - 12.

Gran, S., Olsen, H. & Tellsgård, F. 1976. Hull response to hydrodynamic forces on bow flare. Norwegian Maritime Research, No. 3, pp. 29 - 40.

Greenhow, M. 1987. Wedge entry into initially calm water. Applied Ocean Research, Vol. 9, No. 4.

Greenhow, M. & Yanbao, L. 1987. Added mass for circular cylinders near or penetrating fluid boundaries - review, extension and application to water-entry, -exit and slamming. Ocean Engineering, Vol. 14, No. 4, pp. 325 - 348.

Hooft, J. P. 1970. Oscillating wave forces on small bodies. International Shipbuilding Progress, Vol. 17, No. 188.

Kagemoto, H., Fujino, M. & Okabe, T. 1995. Motions and safety of floating bodies in a wave group. Transactions of the West-Japan Society of Naval Architects, No. 89, March, pp. 91 -102.

Kahma, K., Pettersson, H., Myrberg, K. & Jokinen, H. 1995. Estimated wave conditions and currents during the last voyage of M/S Estonia. Finnish Institute of Marine Research.

Karppinen, T. 1975. Wave-induced motions of semisubmersible drilling rigs. nstm'75 meeting of the Nordic naval architects, Helsinki University of Technology, Finland, 58 p.

de Kat, J. O. & Paulling, J. R. 1989. The simulation of ship motions and capsizing in severe seas. SNAME Transactions, Vol. 97, pp. 139 - 168.

Kalske, S. T., Karppinen, T. O. & Matusiak, J. E. 1985. Arctic mobile drilling structures in waves. 17th Offshore Technology Conference, Paper No. 5033, Houston, May, pp. 107 - 117.

Larsson, L. 1993. Resistance and flow predictions using the SHIPFLOW code. 19th WEGEMT School, Nantes.

Larsson, L., Broberg, L., Kim, K.-J. & Zhang, D.-H. 1990. A method for resistance and flow prediction in ship design. SNAME Transactions, Vol. 98, pp. 495 - 535.

VTT VALMISTUSTEKNIIKKA
Laiva- ja konetekniikka

VTT MANUFACTURING TECHNOLOGY
Maritime Technology

P.O. Box 1705
FIN-02044 VTT
FINLAND

Tel.int.+358 0 4561
Telefax +358 0 455 0619
Telex 122972 vtiha sf

Matusiak, J. & Rantanen, A. 1986. Digital simulation of the non-linear wave loads and response of a non-rigid ship. Proc. CADMO'86, Washington DC, p. 211 - 222.

Newman, J. N. 1977. Marine Hydrodynamics. MIT Press, Cambridge, Massachusetts, 402 p.

Payne, P. R. 1981. The vertical impact of a wedge on a fluid. Ocean Engineering, Vol. 8, No. 4, pp. 421 - 436.

Raff, A. I. 1972. Program SCORES - Ship structural response in waves. Ship Structure Committee Report SSC-230, U.S. Coast Guard Headquarters, Washington D.C. 63 p.

Sundell, T. 1995. MV Estonia accident investigation. Forces on the bow visor due to stationary flow. VTT Manufacturing Technology, Report VALC55, Espoo, January.

Trosch, A.W. & Kang, C.-G. 1988. Evaluation of impact loads associated with flare slamming. SNAME Spring Meeting/STAR Symposium, Pittsburgh, Pennsylvania, June, pp. 117 - 132.

Yamamoto, Y., Fujino, M. & Fukasawa, T. 1980. Motion and longitudinal strength of a ship in head sea and the effects of non-linearities. Naval Architecture and Ocean Engineering, Vol. 18, pp. 91 - 100.